

YY1-controlled regulatory connectivity and transcription are influenced by the cell cycle

Received: 10 November 2023

Accepted: 16 July 2024

Published online: 29 August 2024

Jessica C. Lam  ^{1,2}, Nicholas G. Aboreden ^{1,2}, Susannah C. Midla  ¹, Siqing Wang  ¹, Anran Huang ¹, Cheryl A. Keller  ^{3,4}, Belinda Giardine  ³, Kate A. Henderson ¹, Ross C. Hardison  ³, Haoyue Zhang  ⁵ & Gerd A. Blobel  ^{1,2} 

 Check for updates

Few transcription factors have been examined for their direct roles in physically connecting enhancers and promoters. Here acute degradation of Yin Yang 1 (YY1) in erythroid cells revealed its requirement for the maintenance of numerous enhancer–promoter loops, but not compartments or domains. Despite its reported ability to interact with cohesin, the formation of YY1-dependent enhancer–promoter loops does not involve stalling of cohesin-mediated loop extrusion. Integrating mitosis-to-G1-phase dynamics, we observed partial retention of YY1 on mitotic chromatin, predominantly at gene promoters, followed by rapid rebinding during mitotic exit, coinciding with enhancer–promoter loop establishment. YY1 degradation during the mitosis-to-G1-phase interval revealed a set of enhancer–promoter loops that require YY1 for establishment during G1-phase entry but not for maintenance in interphase, suggesting that cell cycle stage influences YY1's architectural function. Thus, as revealed here for YY1, chromatin architectural functions of transcription factors can vary in their interplay with CTCF and cohesin as well as by cell cycle stage.

The spatial organization of mammalian genomes is dynamic during development^{1,2} and throughout the cell cycle³. Elegant studies elucidated how so-called structural loops form when the cohesin complex extrudes chromatin until halted by two convergent CTCF-bound sites^{4–14}. Degron-based approaches, which prioritize direct over indirect effects, have further informed mechanisms of chromatin loop formation¹⁵. These include acute depletion of RAD21 (refs. 16–23), WAPL^{17,19}, CTCF^{19,20,24,25}, GAF²⁶, BRD4 (refs. 27,28), Mediator^{22,29–32} and Pol II^{33–35} (and drug-induced inhibition of Pol II^{22–24,36,37}). Critically, these perturbations, especially when done acutely, caused only limited, if any, loss of enhancer–promoter (E–P) loops, implying that E–P loops are mediated by yet-to-be-characterized factors. Several transcription factors not directly linked to the CTCF–cohesin machinery have been implicated in E–P looping, including but not limited to Yin Yang

1 (YY1)^{38–50} (for comprehensive reviews, see refs. 51,52). A given E–P loop may rely on multiple factors, as in the case of E–P looping at the β -globin locus, which requires the recruitment of architectural factor LDB1 (refs. 53–57) or the cofactor FOG1 by GATA1 (refs. 56,58). In select cases, such as LDB1 (refs. 56,57,59) and YY1 (ref. 50), gain-of-function experiments in which these factors were tethered to predetermined genomic sites and shown to generate chromatin loops suggest direct action in a loop formation.

In the case of YY1, vastly different architectural outcomes have been reported, ranging from a requirement for the majority of E–P loops to being virtually dispensable for such contacts^{19,50}. Upon YY1 degradation for 24 h in mouse embryonic stem cells (mESCs), YY1–YY1-bound loops decreased genome wide, and several thousand genes were dysregulated⁵⁰. The authors proposed that YY1 forms loops via its

¹Division of Hematology, The Children's Hospital of Philadelphia, Philadelphia, PA, USA. ²Perelman School of Medicine, University of Pennsylvania, Philadelphia, PA, USA. ³Department of Biochemistry and Molecular Biology, Pennsylvania State University, University Park, PA, USA. ⁴Genomics Research Incubator, Pennsylvania State University, University Park, PA, USA. ⁵Institute of Molecular Physiology, Shenzhen Bay Laboratory, Shenzhen, China.

 e-mail: blobel@email.chop.edu

ability to homodimerize^{43,60,61}. Whether YY1 also acts via blockade of cohesin-mediated chromatin loop extrusion is unknown. In contrast, YY1 loss for 3 h in mESCs failed to trigger major alterations to E-P loops or nascent transcription¹⁹, supporting a model in which E-P loops and transcription can be maintained at least temporarily in the absence of YY1.

How YY1 functions mechanistically and the extent of its reliance on other architectural factors are still unresolved. Co-immunoprecipitation experiments^{62–64} suggest that YY1 looping may involve interaction with CTCF^{65,66} and/or cohesin. Another study based on observations in neuronal progenitor cells suggested that YY1-anchored loops form within encompassing CTCF-bound structural loops³⁹.

To identify requirements for de novo E-Ploop establishment, previous studies exploited the dramatic switch from a condensin-driven randomly looped chromatin state to a cohesin-driven looped state during the mitosis-to-G1-phase transition^{24,33,67–70}. *Cis*-regulatory element (CRE) loops can form before CTCF-cohesin-driven structural loops^{67,71} and even in the absence of CTCF²⁴. Thus, many CRE loops are established and maintained independently of CTCF and cohesin.

Discrepancies between the effects of 3-h and 24-h YY1 degradation could reflect differences in cell cycle passage. Acute depletion of architectural factors, specifically during mitosis and G1 phase (from here on referred to as G1 entry), has rarely been performed^{24,33,70,72}. Therefore, we know little about whether conclusions derived from studies using asynchronous (that is, largely interphase) cells can be applied to the mitosis-to-G1 context, and vice versa. Is there a distinction between ‘maintenance’ during interphase versus the ‘establishment’ of loops following mitosis?

Here we used a YY1 degron system in asynchronously growing populations and in cells traversing mitosis-to-G1 to comprehensively survey YY1’s architectural functions. YY1 is required for the maintenance of a subset of CRE loops in interphase and for the establishment of an overlapping yet distinct set of loops after mitotic exit. We propose that the cell cycle serves as a critical layer of regulatory control over when YY1 and possibly other architectural transcription factors regulate chromatin looping and transcription.

Results

Interphase maintenance of a subset of loops requires YY1

Although YY1 was proposed to be a general E-P looping factor⁵⁰, acute depletion has only been performed in pluripotent cells^{19,50}, which may be more robust to YY1 knockout^{64,73}. Also, whether the distinctively short G1 phase⁷⁴ of pluripotent cells impacts their chromatin structuring mechanisms remains unknown. Therefore, we examined YY1’s role in maintaining chromatin structure in G1E-ER4 cells⁷⁵, a mouse erythroblast line dependent on YY1 for long-term growth (Extended Data Fig. 1a).

We created a YY1 auxin-inducible degron (YY1-AID) subline for rapid degradation of the YY1 protein (Fig. 1a). Western blot and chromatin immunoprecipitation followed by sequencing (ChIP-seq) confirmed efficient YY1 degradation and removal from chromatin after 4-h auxin treatment (Fig. 1b,c and Extended Data Fig. 1b–e). YY1 ChIP-seq also revealed its localization at active enhancers and promoters, as previously reported⁵⁰ (Fig. 1d). Even acute degron systems may not entirely

exclude secondary effects. RNA sequencing (RNA-seq) confirmed that the mature mRNA pool is still largely stable after 4-h auxin treatment, suggesting that the consequences of YY1 depletion described below are not secondary to changes in most known architectural factors, including CTCF and cohesin, whose transcript levels remained unchanged (Supplementary Fig. 1a–c). However, prolonged YY1 depletion for 24 h dysregulated 2,663 genes, which may be a consequence of both primary and secondary effects (Supplementary Fig. 1b).

We investigated chromatin structure via Micro-C^{36,76} of interphase-predominant, asynchronously growing cells after 4-h YY1 degradation. We called loops with the software cooltools^{9,77} and defined changes based on ≥ 1.5 -fold differences in loop strength (observed over locally-adjusted expected contacts). We expect this approach to capture higher-confidence YY1-dependent loops for further characterization, although smaller looping changes may still impact transcription^{78–80}. In total, we detected 12,738 loops across –auxin and +auxin conditions (Extended Data Fig. 2a,b). YY1 depletion in asynchronous cells weakened 1,990 loops, 22% of –auxin-detected loops (Fig. 1e). We also observed 1,591 strengthened loops. Whether YY1 directly suppresses these loops or whether the loss of YY1-dependent loops enables new, perhaps competing contacts, is unclear. While some weakened and strengthened loops might also be due to secondary effects, this seemed unlikely in light of the minimal differences in mRNA levels from the RNA-seq experiments upon 4-h YY1 depletion.

Looping changes occurred despite stable genome-wide contact decay (Extended Data Fig. 1f), compartmentalization (Extended Data Fig. 1g–i) and domain insulation (Extended Data Fig. 1j–m). We also confirmed that loop changes in either direction were unbiased toward weaker loops (Extended Data Fig. 2c,d). Thus, YY1 is required for the maintenance of a substantial fraction of chromatin loops in asynchronously growing mouse erythroblasts but has little impact on compartments and domains within a 4-h time frame.

YY1-dependent CRE loops are often dually anchored by YY1

We broadly categorized loops in the following sequential manner: (1) ‘CRE loops’ if both loop anchors were occupied by H3K27ac-marked promoters or enhancers within a 10 kb window, irrespective of CTCF-cohesin occupancy; (2) ‘structural loops’ if dually anchored by CTCF-cohesin co-occupied sites but possessing 0 or 1 CRE-occupied anchors and (3) ‘uncategorized loops’ for remaining loops.

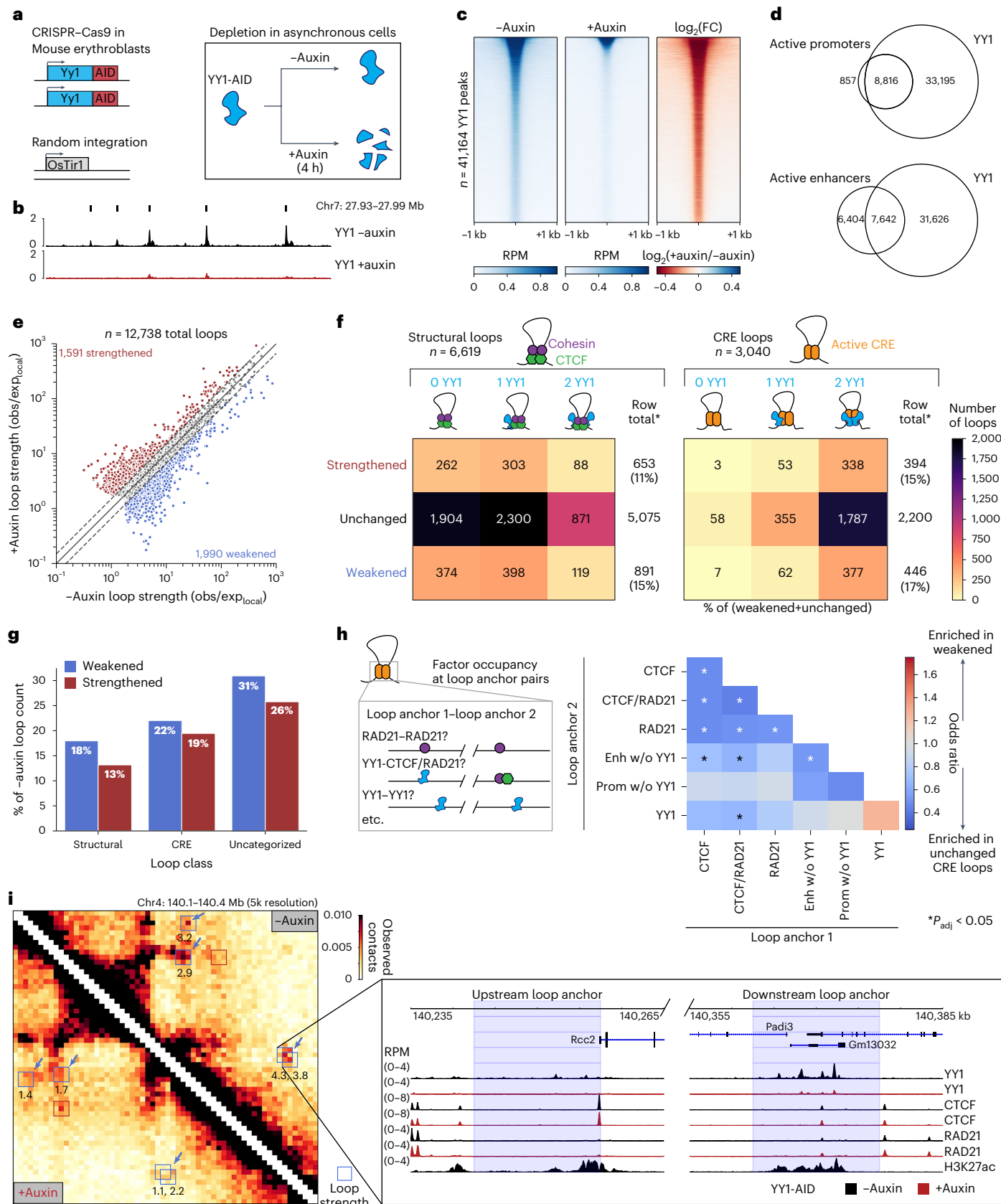
Unexpectedly, YY1 loss impacted loops across all categories. In total, 446 of 3,040 CRE loops were weakened, 439 (98.4%) of which exhibit YY1 binding in at least at one anchor (Fig. 1f). However, 2,142 singly or doubly YY1-anchored loops remained unchanged, suggesting that YY1 is not involved in looping at all sites to which it binds, reminiscent of how only a fraction of CTCF pairs form structural loops^{9,81}, or that those loop changes fell below threshold levels. Notably, 18% of structural loops and 31% of uncategorized loops were weakened in the absence of YY1, most of which had 0 or 1 anchor bound by YY1 (Fig. 1f,g and Extended Data Fig. 2e). Thus, assuming low levels of false-negative ChIP signals, YY1 loss can indirectly trigger changes in structural loops. Given the short duration of YY1 depletion and unaffected progression through mitosis (see below), the broad changes in loop formation are not attributable to shifts in cell cycle profiles.

Fig. 1 | YY1 binding is necessary for the maintenance of CRE loops in asynchronous cells. **a**, Strategy for engineering a YY1-AID system and acutely depleting YY1 in asynchronous cells. **b**, YY1 ChIP-seq tracks from –auxin and +auxin conditions. Rectangles above tracks indicate peak calls ($n = 3$ biological replicates). **c**, Heatmaps of YY1 ChIP-seq signal and $\log_2(FC)$ after 4-h YY1 depletion in asynchronous cells, centered on all YY1 peaks and ordered by –auxin peak strength ($n = 3$ biological replicates). **d**, Venn diagrams of the overlap between active promoters and YY1 peaks (top) and active enhancers and YY1 peaks (bottom). **e**, Scatter plot of loop strength in –auxin and +auxin conditions ($n = 3$ biological replicates). **f**, Table of loop counts, stratified by loop class, loop

change and YY1 occupancy. **g**, Numbers of changed loops across different loop classes, expressed as a percentage of the total number of loops called in –auxin. **h**, Schematic representation illustrating examples of patterns of factor occupancy at paired loop anchors (left). Heatmap showing enrichment of different patterns of factor occupancy in weakened CRE loops versus unchanged CRE loops (right). * $P_{adj} < 0.05$, two-sided Fisher’s exact test, Benjamini–Hochberg multiple testing correction. **i**, Contact maps from –auxin and +auxin samples with blue arrows/boxes indicating examples of weakened loops and the red box indicating a strengthened loop. Tracks show ChIP-seq from –auxin and +auxin conditions, with highlighted regions corresponding to loop anchors. FC, fold change.

Considering the 10 kb window size of loop anchors, the mere presence of a factor within that window does not necessarily indicate a looping function. We therefore classified binding patterns that distinguished YY1-dependent CRE loops from unchanged ones.

YY1-YY1 was the only enriched pattern but did not reach statistical significance, suggesting that other unknown features or cofactors distinguish YY1-dependent loops from the loops where YY1 is bound but not serving a looping function (Fig. 1h). Loop pileups from merged



and replicate contact maps confirmed that YY1-dependent CRE loops were YY1-centered punctate interactions that diminished upon auxin treatment (Extended Data Fig. 2f,g and Supplementary Fig. 3). Homotypic CTCF–CTCF and RAD21–RAD21 pairings or heterotypic YY1–CTCF and YY1–RAD21 pairings were uncommon in YY1-dependent CRE loops (Fig. 1h). The infrequency of these configurations suggests that CTCF-cohesin occupancy is nonessential for YY1 looping.

CRE loops strengthened upon YY1 depletion exhibited heterogeneous, promoter-anchored configurations (Extended Data Fig. 2h). We speculate that loss of YY1-dependent loops may free promoters to interact with regions normally less preferred. Alternatively, YY1 loss may allow other factors to bind promoters and form new loops. In sum, YY1 binding at loop anchors is necessary for the maintenance of numerous CRE loops, especially those bilaterally bound by YY1.

YY1 directs loops independently of CTCF and cohesin stalling

It has been suggested that YY1 may function by stalling cohesin-mediated loop extrusion in a manner analogous to CTCF^{39,50}. Additionally, YY1 may influence looping by modulating CTCF or cohesin binding^{62–64,82,83}. We performed CTCF and RAD21 ChIP-seq and observed 7,931 YY1–RAD21 co-occupied sites (of 41,163 YY1 and 39,745 RAD21 peaks) and 5,968 YY1–CTCF co-occupied sites (of 59,032 CTCF peaks) in untreated cells (Fig. 2a). Reported colocalizations of YY1–CTCF or YY1–cohesin may be present in certain contexts but are much less common than CTCF–cohesin overlap.

Notably, on YY1 depletion, CTCF and cohesin binding was preserved at all sites (Extended Data Fig. 3a,b), including those directly overlapping with YY1 (Figs. 1i and 2b,c). Conversely, YY1 occupancy was also preserved upon CTCF depletion (Extended Data Fig. 3e). Given that YY1 had minimal influence on CTCF and cohesin binding, we also considered the possibility that YY1 could be directing loops through other mechanisms such as recruiting LDB1, another major architectural factor that connects CREs (in preparation). However, ChIP-seq revealed that LDB1 binding was robust to YY1 loss (Extended Data Fig. 3c). Acute alteration to enhancer activities could be another indirect mechanism underlying loop changes. Measuring H3K27ac levels as a surrogate for enhancer strength, we found that the mark was preserved at all H3K27ac ChIP-seq peaks upon YY1 loss, including those located within loop anchors (Extended Data Fig. 3d). Thus, YY1 forms loops without altering CTCF or LDB1 localization, enhancer strength or cohesin stalling. The absence of discernable changes in cohesin peaks at YY1-overlapping sites excludes a model in which YY1 acts as an extrusion blocker. YY1 dimerization^{43,48,50,60,61} remains the most parsimonious model of CRE looping, yet we cannot discount the possibility that YY1 also interacts with yet-to-be-identified partners in heterotypic contacts.

Extrusion intermediates may promote YY1-mediated looping

It remains possible that cohesin-mediated extrusion facilitates loop formation by juxtaposing CREs that are subsequently stabilized by YY1. Alternatively, YY1-bound loop anchors may connect through

the random movement of chromatin. To characterize the CTCF- and cohesin-dependence of YY1-dependent loops, we integrated loop changes from multiple degrons—YY1–AID (this study), CTCF–AID²⁴ and SMC3–AID⁸⁴. Structural loops were almost completely lost upon CTCF or cohesin depletion, as expected (Fig. 2d,f and Extended Data Fig. 3f). In contrast, YY1-dependent CRE loops showed only partial decreases in loop strength upon CTCF or cohesin loss (Fig. 2e,g). CRE loops that do not rely on YY1 showed a slightly greater reduction in loop strength in CTCF- or cohesin-depleted cells (Extended Data Fig. 3g-i), in line with the idea that YY1-dependent loops are less likely to rely on structural loop factors than other CRE loops. Notably, YY1-dependent CRE loop strengths show much greater reliance on YY1 than on cohesin (Extended Data Figs. 3j and 4a,b).

As evidenced in aggregate peak analysis plots, loop strength upon cohesin degradation is confounded by a general reduction in signal, including that surrounding the focal loop anchor sites. To distinguish focal changes from broader reductions in contacts, we measured contact frequencies at different radii from the loop center (Fig. 2h). Structural loops exhibited the strongest reduction of contacts near the centers of the loop anchors relative to regions more distal to the loop centers, consistent with cohesin being locally stabilized at CTCF sites (Fig. 2i). In contrast, in the case of YY1-dependent loops, reduction in contacts was spread evenly over segments outside of the loop centers (Fig. 2j). Accordingly, 43% of detected YY1-dependent CRE loops showed this pattern of broad contact loss but maintained focal contact in the absence of cohesin (Fig. 2k). Thus, a fraction of YY1-dependent CRE loops, although not focal cohesin stalling points, may still be affected by cohesin as part of an extrusion process. One qualification is that our conclusions pertain to loop calls greater than 45 kb in length. Because smaller loops reportedly tend to be less reliant on cohesin^{19,20,79,85,86}, the fraction of YY1-dependent, cohesin-independent loops may be greater. Among the called ≥45-kb CRE loops, cohesin-dependent CRE loops were comparable in length to other CRE loops (Extended Data Fig. 4c,d).

Integrating findings from multiple perturbations and ChIP-seq experiments, we propose a model in which YY1 directs the specificity of contacts between loop anchors, whereas cohesin tunes contact frequency across broad regions without directed action at the YY1 loop anchors (Fig. 2l). Without YY1, extrusion intermediates exist but sustained contacts cannot form, and without cohesin, extrusion intermediates fail to form, resulting in reduced YY1 contact frequencies.

YY1 activates transcription in a dose-dependent manner

YY1 has been reported to function as a transcriptional activator and repressor^{87–90}. However, its widespread requirement for transcription, at least on a short timescale, has been disputed¹⁹. We performed total Pol II ChIP-seq following 4-h YY1 depletion and measured Pol II levels in gene bodies as a reflection of active transcription (Extended Data Fig. 5a,b). Surprisingly, 959 of 9,465 active genes were downregulated, whereas only two were upregulated greater than 1.5-fold (Fig. 3a). While

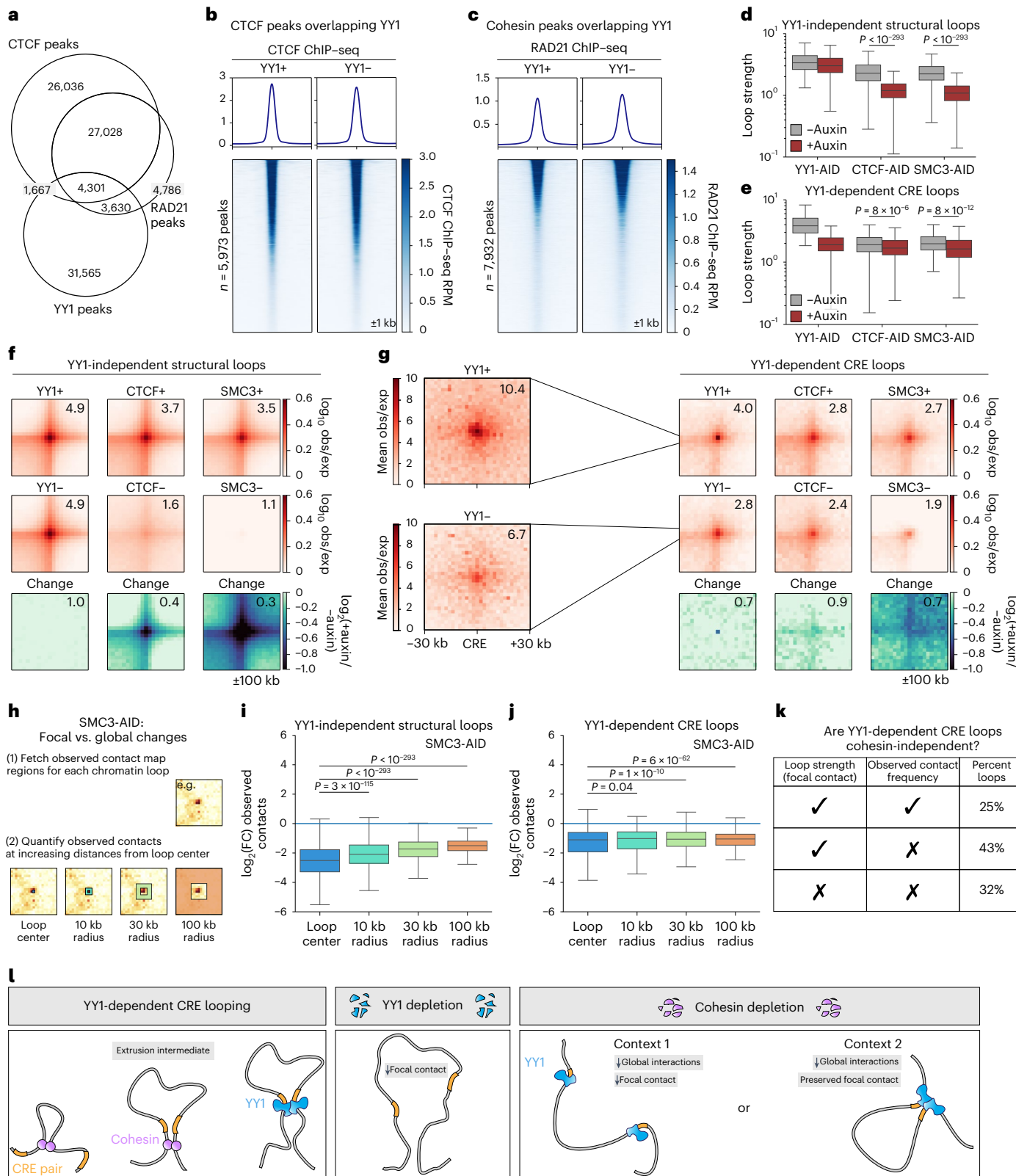
Fig. 2 | YY1-anchored loops can form independently of CTCF and cohesin.

a, Venn diagram of CTCF, RAD21 and YY1 ChIP-seq peaks from asynchronous, untreated YY1–AID cells. **b**, Heatmap showing CTCF ChIP-seq peak signal before and after YY1 depletion ($n = 2$ biological replicates). The signal is centered on CTCF peaks, which overlap with YY1. **c**, Heatmap showing RAD21 ChIP-seq peak signal before and after YY1 depletion ($n = 2$ biological replicates). The signal is centered on RAD21 peaks, which overlap with YY1. **d**, Box plot of loop strengths of YY1-independent structural loops after YY1, CTCF or SMC3 degradation (two-sided Mann–Whitney *U* test; $n = 5$ biological replicates for YY1–AID, $n = 2$ for CTCF–AID and SMC3–AID; $n = 4,895$ loops). **e**, Box plot of loop strengths of YY1-dependent CRE loops after YY1, CTCF or SMC3 degradation (two-sided Mann–Whitney *U* test; $n = 5$ biological replicates for YY1–AID, $n = 2$ for CTCF–AID and SMC3–AID; $n = 440$ loops). **f**, Pileup plots of YY1-independent structural loops, based on observed/expected signal from 10k resolution YY1–AID, CTCF–AID and

SMC3–AID contact maps. **g**, Pileup plots of YY1-dependent CRE loops, based on observed/expected signal from 1k resolution YY1–AID (left) and 10k resolution YY1–AID, CTCF–AID and SMC3–AID contact maps (right). **h**, Schematic representation of the approach to quantifying observed contacts within and surrounding loops. **i**, $\log_2(\text{FC})$ of observed contacts within and surrounding YY1-independent structural loops (two-sided Mann–Whitney *U* test; $n = 4,895$ loops). **j**, $\log_2(\text{FC})$ of observed contacts within and surrounding YY1-dependent CRE loops (two-sided Mann–Whitney *U* test; $n = 440$ loops). **k**, Table of the percentages of YY1-dependent loops with loop strength and/or observed contact frequency dependent on cohesin. **l**, Model of YY1-dependent CRE looping (left), how focal contacts are lost without YY1 (middle) and how the loss of extrusion intermediates can weaken some YY1-dependent CRE loops while some YY1-bound CREs can still connect through random movement of chromatin (right).

Pol II ChIP-seq revealed YY1's positive influence on Pol II binding, YY1 might additionally affect other variables that affect transcriptional output, such as Pol II elongation speed or cotranscriptional processes. We considered these additional layers of regulation by performing TT-seq^{9,10}, an approach to measure nascent transcription via metabolic labeling of RNA. Spike-in normalized TT-seq also revealed that YY1 serves predominantly as a transcriptional activator (Supplementary Fig. 1b).

Fig. 2). Thus, YY1 is necessary for the short-term maintenance of active transcription and may do so by promoting E-P contacts or recruiting transcriptional machinery to gene promoters. In contrast, YY1 is either mostly dispensable for direct silencing of transcription^{9,10} or may be required for initial gene repression but dispensable thereafter due to epigenetic factors that maintain gene silencing^{9,10}. Late (24 h) upregulation of genes (Supplementary Fig. 1b) may also simply



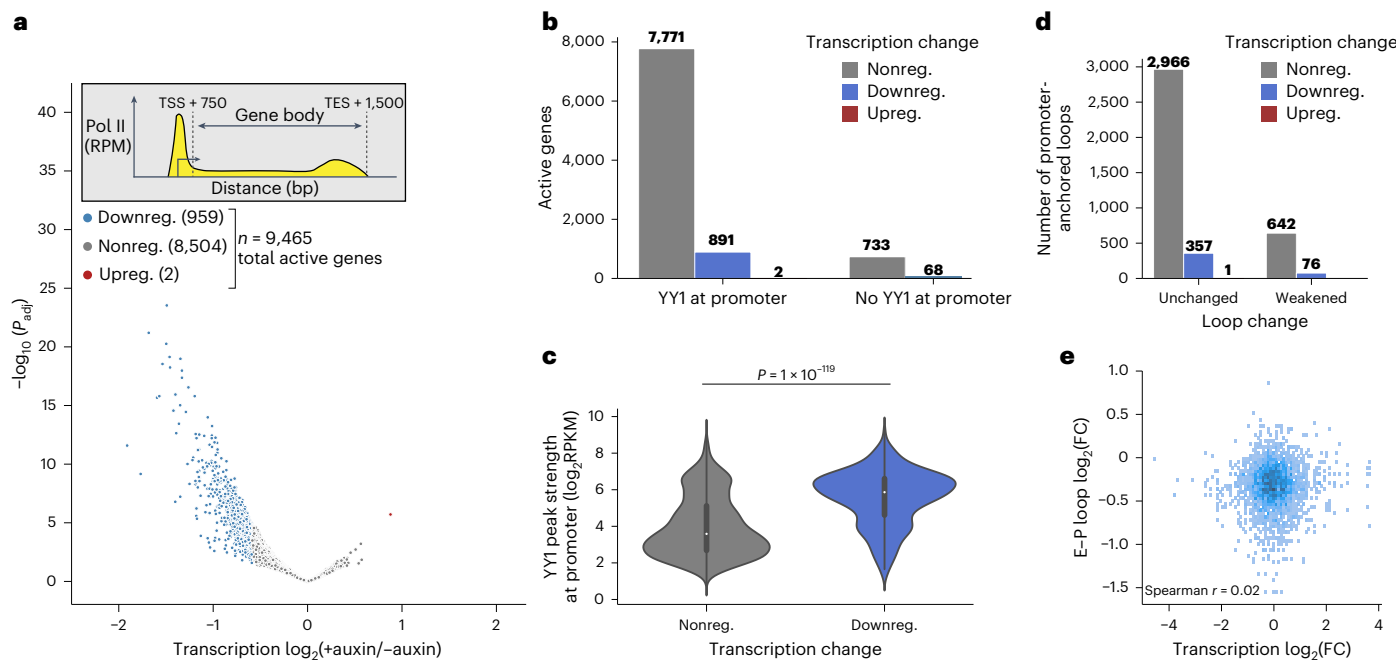


Fig. 3 | Promoter-proximal YY1 binding drives YY1-dependent transcription in asynchronous cells. **a**, Volcano plot of changes in total Pol II signal in gene bodies following YY1 depletion in asynchronous cells ($n = 3$ biological replicates). Inset, a cartoon depicting how gene body was defined (TSS: transcription start site, TES: transcription end site). **b**, Bar plot of the numbers of active genes with YY1 binding at the promoter, stratified by their differential expression following

depletion of YY1. **c**, Violin plot of YY1 ChIP-seq peak strength at the promoter of nonregulated active genes versus downregulated active genes (two-sided Mann–Whitney *U* test). **d**, Bar plot showing the number of CRE loops associated with each category of transcription change. **e**, Scatter plot showing transcription changes versus E–P loop changes after YY1 depletion.

reflect that derepression occurs more gradually than the loss of active transcription.

Most active gene promoters (8,664 of 9,465) exhibited detectable YY1 binding, including 891 of 959 downregulated genes (Fig. 3b). Genes that were downregulated tended to harbor stronger YY1 peaks (Fig. 3c), and the degree of YY1 dependence correlated with YY1 peak strength (Extended Data Fig. 5c). Hence, the necessity of YY1 for maintenance of transcription is partly informed by its binding intensity at promoters.

Transcription and looping can be uncoupled

In addition to exerting promoter-proximal effects, YY1 may activate genes by promoting CRE loops. We observed that 76 of 718 YY1-dependent CRE loops overlapped with downregulated genes (Fig. 3d). When focusing on E–P loops within the CRE loop class, loop loss and transcriptional reduction were uncorrelated (Fig. 3e). One complicating aspect is that genes can loop to multiple CREs, and vice versa (Extended Data Fig. 5d,e). We observed that 40% of genes associated with a YY1-dependent loop also overlapped with YY1-independent CRE loops. Gene activity could appear decoupled from looping if YY1-independent loops, including smaller ones we may miss on Micro-C, compensate for the loss of individual YY1-dependent loops.

Another possibility is that some genes may be predominantly regulated through promoter-proximal effects, which would mask the effects of distal regulation when considering all genes. When focusing on a small subset of genes without promoter-bound YY1, downregulation was slightly more pronounced for genes looped to a YY1-bound distal enhancer (Extended Data Fig. 5f), although the effect size was still uncorrelated with E–P looping changes (Extended Data Fig. 5g).

Conversely, there have been varying reports of the influence of transcription and Pol II occupancy on CRE loops^{22,23,30,33–37,95}. Therefore, it is also possible that YY1 loss-induced reduction of Pol II occupancy (Extended Data Fig. 5h) affects CRE loop stability.

In sum, at a timescale of 4 h and within a single cell cycle, loss of CRE loops may be uncoupled from transcriptional changes, with the

important caveat that individual genes may possess different sensitivities to distal regulation^{78–80}.

Select promoters exhibit mitotic retention of YY1

While YY1 maintains a fraction of chromatin loops and the activity of a subset of genes, many YY1-bound loops and genes remain unaffected by acute YY1 loss in asynchronous cells. This raises the question of whether YY1 binding may be more critical when chromatin structure and transcription are built from the ground up, such as during the mitosis-to-G1 transition^{68,69,96,97}. During mitosis, YY1 is mostly removed from chromatin^{98–100}. It remains untested whether partial YY1 retention on mitotic chromatin, as observed by imaging¹⁹, localizes to specific genomic sites. Because YY1 retention and recruitment dynamics may affect chromatin loop establishment, we performed YY1 ChIP-seq on synchronized, fluorescence-activated cell sorting (FACS)-purified populations (Methods) at the following five stages during the mitosis-to-G1 interval: prometaphase, anaphase/telophase, early G1, mid G1 and late G1 (Fig. 4a and Extended Data Fig. 6a,b).

YY1 chromatin occupancy increased as cells transitioned from prometaphase to G1 but at markedly different rates for individual sites (Fig. 4b,c). We detected 681 YY1 peaks in mitotic chromatin (Fig. 4d). Prometaphase YY1 retention was validated at eight sites via input-normalized ChIP-qPCR. YY1 binding was lower in mitotic chromatin but correlated with interphase signal strength (Extended Data Fig. 6c). We conducted in silico simulations to exclude interphase contamination as the source of prometaphase signal (Extended Data Fig. 6d,e). Mitotic chromatin accessibility, based on published DNase-seq¹⁰¹, was similar in retained versus nonretained YY1 sites (Fig. 4e).

In total, 5,713 peaks were detected as early as anaphase/telophase, and most sites were re-occupied by early G1 (Fig. 4d). Stratifying sites by the time of YY1 detection, we observed that retained and rapidly recruited sites were more likely to have strong YY1 motifs (Fig. 4f,g). Notably, YY1 retention was strongly biased toward promoter regions,

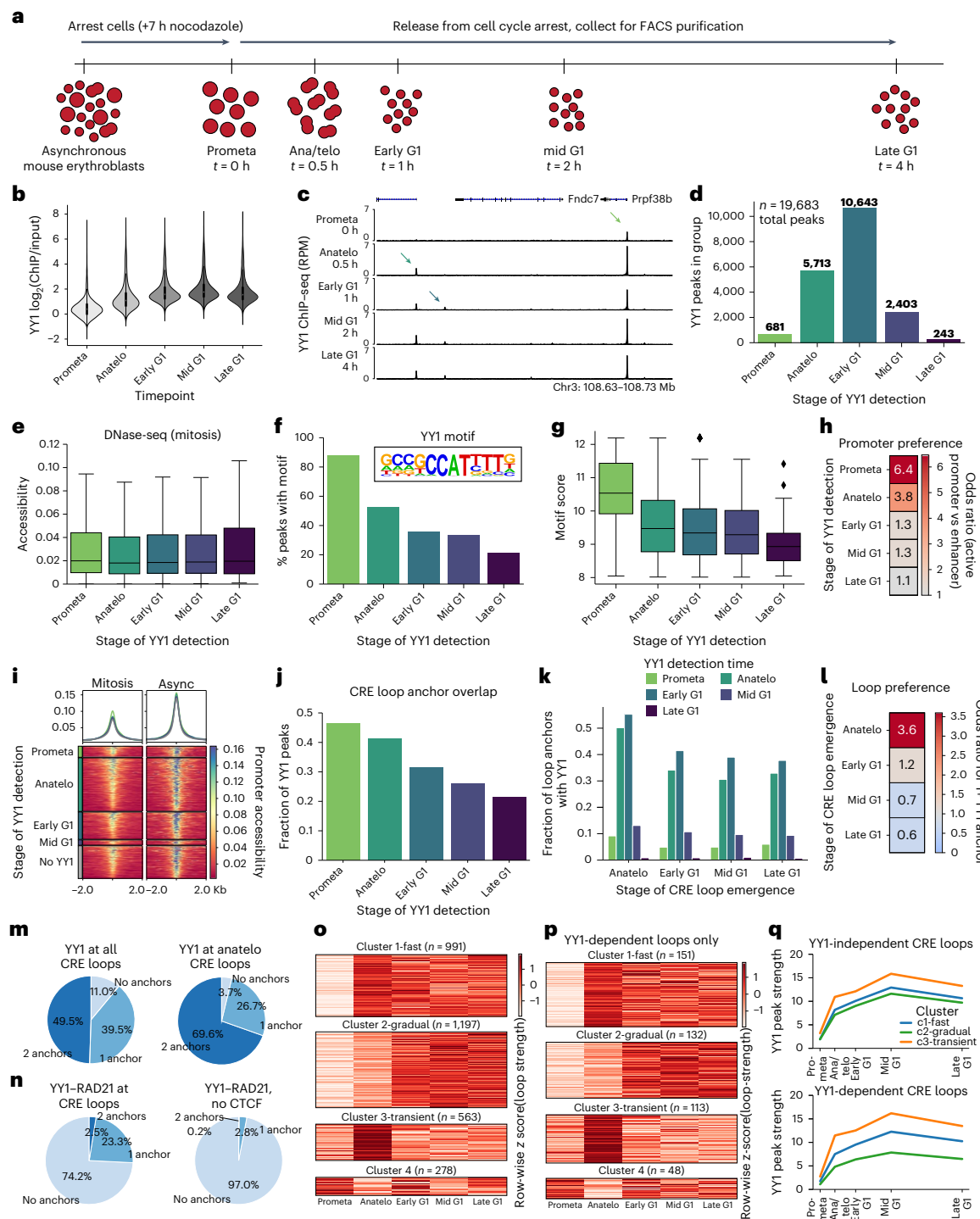


Fig. 4 | YY1 is partially retained on mitotic chromatin and rapidly recruited to CRE loop anchors during G1 entry. **a**, Schematic representation illustrating the approach to purifying cells at different stages of the mitosis-to-G1 transition. **b**, Violin plot of YY1 ChIP-seq signal at each timepoint across all YY1 binding sites ($n = 3$ biological replicates). **c**, YY1 ChIP-seq tracks across cell cycle stages. Arrows indicate peaks detected at different mitosis-to-G1 stages. **d**, Bar plot of the new peaks detected at each mitosis-to-G1 stage. **e**, Box plot of chromatin accessibility in mitosis for YY1 peaks, stratified by peak detection time. **f**, Bar graph of the percent of YY1 peaks overlapping with a YY1 motif (inset), stratified by peak detection time. **g**, Box plot of the motif scores associated with motif-containing YY1 peaks, stratified by peak detection time. **h**, Enrichment of active promoters relative to active enhancers overlapping with YY1 peaks. **i**, Heatmap of chromatin accessibility centered on promoter-associated YY1 peaks. **j**, Bar plot depicting

fraction of YY1 peaks that overlap with CRE loop anchors. **k**, Bar plot depicting fraction of CRE loop anchors that contain YY1 peaks, stratified by YY1 detection time. **l**, Enrichment of YY1 binding, at either one or both anchors, at CRE loops that emerge at different timepoints. **m**, Pie charts of YY1 occupancy at all CRE loops (left) and at CRE loops that emerge at anaphase/telophase (right). **n**, Pie charts of CRE loops that are occupied by YY1-RAD21 cobound (left) and those exclusively occupied by YY1-RAD21 (right). **o**, Heatmap showing clusters of loop dynamics across the mitosis-to-G1 interval. Each row represents each loop, and each column represents one stage. **p**, Same as o, except only the loops that are dependent on YY1 in asynchronous cells. **q**, Line plots showing averaged YY1 ChIP-seq peak strengths throughout the mitosis-to-G1 transition for peaks overlapping with each CRE loop cluster.

although promoters had comparable accessibility regardless of YY1 dynamics (Fig. 4*h,i*).

In sum, YY1 is largely displaced from mitotic chromosomes and rebinds rapidly as cells enter G1. This transition enables investigation of how dynamics of YY1 loop formation relate to YY1 re-occupancy.

YY1 retention and early binding occur at CRE loop anchors

Because CRE loops appear as early as anaphase/telophase, they are likely established by retained or rapidly recruited factors other than the cohesin machinery, which accumulates later in G1 (ref. 67). However, the influence of transcription factor retention and recruitment kinetics on CRE loop formation has not yet been explored, other than for CTCF²⁴. To investigate this, we intersected YY1 ChIP-seq with our previously published, stage-matched Hi-C maps⁶⁷.

Retained and early bound YY1 sites frequently resided in CRE loop anchors (Fig. 4*j*). CRE loop anchors displayed the strongest gains in YY1 occupancy at anaphase/telophase or early G1, irrespective of when the loop was detected (Fig. 4*k*). From a ‘loop-centric’ view, anaphase/telophase-detected CRE loops, relative to later-forming ones, were most likely to be occupied by YY1, and 69.6% exhibited binding at both loop anchors (Fig. 4*l,m*). Only 0.2% of CRE loops exhibited YY1-RAD21 cobinding at both anchors during the mitosis-to-G1 transition (Fig. 4*n*).

In sum, we observed concordant YY1 re-occupancy and loop detection at certain loci, consistent with a role for YY1 in the formation of these loops. However, YY1 occupancy frequently precedes loop detection, implicating an additional limiting step in loop formation. Discrepancies between when YY1 binding and looping are detected could also be due to differences in ChIP-seq versus Micro-C sensitivity. Alternatively, some YY1-flanked loops may not require YY1 for their establishment. This question is addressed below with a mitotic YY1 degradation approach.

YY1-bound loops can form rapidly after mitotic exit

To study the establishment dynamics of YY1-dependent CRE loops, we first selected loops that had already been identified as YY1-dependent in asynchronous cells. As in previously reported Hi-C studies^{24,67}, *k*-means clustering of all CRE loops revealed fast-forming loops at anaphase/telophase, transient loops that peaked at anaphase/telophase and gradually forming loops (Fig. 4*o*). YY1-dependent CRE loops were more likely to form faster (Fig. 4*p*).

Both fast loops and gradual loops continued to gain YY1 binding into G1, although fast loops reached maximum loop strength in anaphase/telophase (Fig. 4*q*). Loops requiring YY1 during interphase gained YY1 binding at their anchors regardless of loop dynamics but exhibited varying levels of YY1 (Fig. 4*q*). Gradual-forming loops had lower levels of YY1 beginning at anaphase/telophase and into G1. Thus, we hypothesize that threshold levels of YY1 at anaphase/telophase, rather than final levels in interphase, may enable loop establishment. To determine a causal role for YY1 re-occupancy in loop establishment and transcription, we proceeded to deplete YY1 during the mitosis-to-G1 transition.

Some CRE loops require YY1 exclusively during G1 entry

Depletion of YY1 in asynchronous cells may have missed YY1-dependent features that could be maintained by other factors. Also, re-organization of YY1-dependent structures may require progression through mitosis, as has been shown for other architectural reconfigurations^{25,102–104}. Therefore, we depleted YY1 during mitosis and into mid G1 to investigate its requirement for the establishment of chromatin loops during mitotic exit. Following synchronization and YY1 depletion, cells were FACS-purified and studied by Micro-C (Fig. 5*a*). YY1 chromatin occupancy was undetectable by ChIP-qPCR confirming its depletion (Extended Data Fig. 7*a*). FACS-based assessment of cell populations confirmed that G1 entry proceeded normally upon acute depletion of YY1 (Extended Data Fig. 7*b*). Additionally, Micro-C contact decay

curves, as well as the formation of compartments and domains, were the same in control and YY1-depleted cells (Extended Data Fig. 7*c–i*).

At mid G1 (2 h after mitotic release), a total of 14,155 chromatin loops were called. Two thousand six hundred and ninety chromatin loops failed to establish normally, and 2,487 chromatin loops were strengthened when compared to controls (Fig. 5*b*). Stratifying by loop class, we observed that 30% of CRE loops failed to achieve their normal strength (Fig. 5*c* and Supplementary Fig. 4). Thus, depletion of YY1 during the mitosis-to-G1 transition revealed a greater absolute number and fraction of weakened CRE loops than in asynchronous cells. However, absolute loop counts should be interpreted with caution given that synchronized mid G1 cells represent different biological states than asynchronous cell populations. There were also additional strengthened loops across loop classes (Fig. 5*c*). We speculate that a transient absence of competing loops or competing factors may make the mitosis-to-G1 transition distinctively conducive to the formation of new loops.

Early YY1 recruitment enables the establishment of CRE loops

After identifying loops dependent on YY1 for establishment, we revisited the relationship between the kinetics of YY1 re-occupancy and looping during the mitosis-to-G1 transition. YY1-dependent loops with YY1 present on both anchors emerged at anaphase/telophase, consistent with the anaphase/telophase YY1 re-occupancy (Fig. 5*d–f*).

We again used two approaches to measure looping-loop strength to capture focal contact and observed contact frequency to reflect broader changes in interactions. Observed contacts progressively increased after mitotic exit (Fig. 5*g*). However, loop strength stabilized at anaphase/telophase (Fig. 5*h*). This pattern of preserved loop strength (observed over locally-adjusted expected contacts) but changed observed contacts (not adjusted for the local background) echoes what was observed in the cohesin degron. Anaphase/telophase may represent a cohesin-depleted state in which YY1-dependent loops can form, whereas G1 is a cohesin-replete state when extrusion broadly increases long-range interactions.

We observed a weak positive correlation between YY1 ChIP-seq peak strength and YY1–YY1 loop reformation (Fig. 5*i*). Loop strength increased with YY1 binding until a certain threshold, at which it plateaued regardless of further increasing peak strength. This could indicate that inhibitory features—such as extrusion-induced constraints on chromatin mobility¹⁰⁵, emergence of domain boundaries or formation of interfering loops—prevent additional gains in loop strength in G1. Alternatively, YY1 peak strength may only affect loop strength up to a point at which other (co-)factors become rate-limiting.

Uncoupling of gene re-activation from CRE looping

Conflicting evidence exists regarding an immediate causal relationship between transcription and chromatin looping^{106,107}. We wondered whether a stronger correlation emerges when cells re-initiate looping and transcription after mitosis. Alternatively, the nonspecific hyperactivity of the genome¹⁰⁸ immediately following mitosis may supplant distal regulation.

To identify genes dependent on YY1 for re-activation, we performed Pol II ChIP-seq on early, mid and late G1 samples after mitosis-to-G1 depletion of YY1. The number of downregulated genes (Fig. 6*a*) and the degree of downregulation of YY1-dependent genes (Fig. 6*b*) increased with G1 progression. Genes bound by YY1 in pro-metaphase and anaphase/telophase exhibited more rapid and extensive downregulation (Fig. 6*c*). This trend suggests that transcriptional re-activation after mitosis is initially robust, but rapid YY1 re-occupancy at promoters is required to maintain active transcription in late G1.

We next examined whether the reduction in transcription was associated with lost E-P loops during mid G1. Most E-P loops associated with downregulated genes were unchanged in the absence of YY1 (Fig. 6*d,e*). Thus, even in the context of gene re-activation after mitosis, E-P looping may be uncoupled from transcription. Proposed models

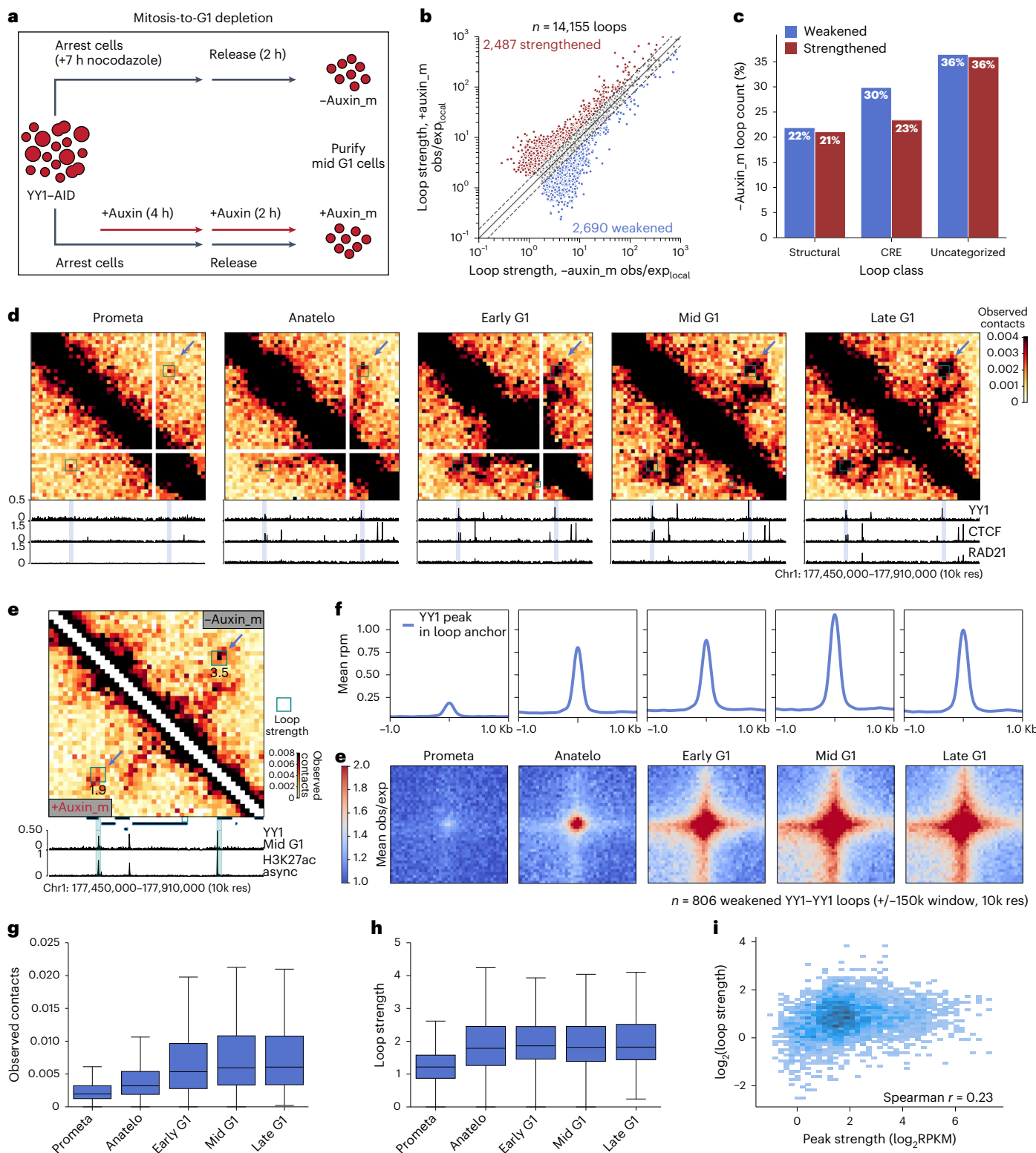


Fig. 5 | YY1 recruitment dynamics and requirements for CRE loop establishment during the mitosis-to-G1 transition. **a**, Experimental approach to mitosis-to-G1 depletion of YY1. **b**, Scatter plot of loop strengths in -auxin_m and +auxin_m samples for all loops detected in mid G1. **c**, Percent of loops changed within each loop class, expressed as a percentage of the loops called in the -auxin_m condition. **d**, Hi-C contact maps at mitosis-to-G1 stages showing the formation of a YY1-dependent loop (blue arrow), with stage-matched ChIP-seq tracks of YY1, CTCF and RAD21. **e**, Effects of mitosis-to-G1 depletion on the

YY1-dependent loop depicted in **d** (blue arrow). **f**, Pileup plots of YY1-dependent loops based on mitosis-to-G1 Hi-C maps in the parental cell line (bottom) and the YY1 peaks located in their loop anchors (top). **g**, Box plot showing observed contacts of YY1-dependent loops that are included in the pileups in **f**. **h**, Box plot showing loop strengths of YY1-dependent loops that are included in the pileups in **f**. **i**, Scatter plot of YY1 peak strengths and associated loop strengths for YY1-dependent loops that are included in the pileups in **f**.

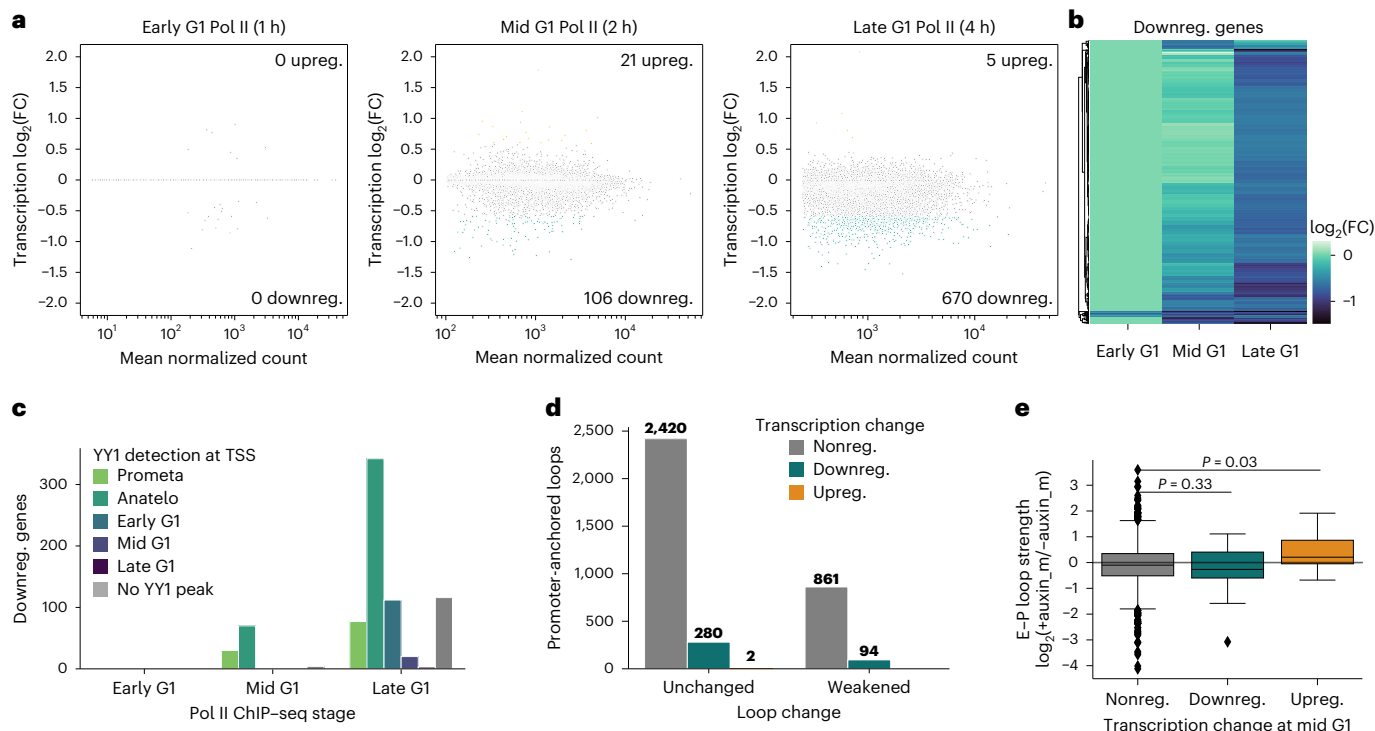


Fig. 6 | Transcriptional kinetics in G1 entry after depletion of YY1. a, a, Scatter plots showing $\log_2(\text{FC})$ in gene body Pol II signal in early, mid and late G1 after YY1 depletion in the mitosis-to-G1 phase interval. b, Heatmap of $\log_2(\text{FC})$ for genes downregulated following mitosis-to-G1 depletion of YY1. Each row represents one gene. c, Bar plot of numbers of downregulated genes at each timepoint that

has a YY1 ChIP-seq peak at the promoter, stratified by time of YY1 detection. d, Bar plot of the number of genes associated with weakened CRE loops versus unchanged CRE loops, stratified by the genes' YY1 dependence. e, Box plot of E-P loop changes associated with nonregulated, downregulated and upregulated genes (two-sided Mann-Whitney *U* test).

of nonlinear effects^{78,80} or time-buffered effects¹⁹ of chromatin looping on transcription may also apply when cells traverse mitosis.

Cell cycle stages modulate requirements for CRE looping

A previous HiChIP study reported massive changes in E-P looping after 24-h YY1 depletion⁵⁰. Generally, loop perturbations may be accentuated by passage through multiple cell cycles in this time frame. However, systematic comparisons between looping changes in interphase depletion versus mitotic depletion in the same cell line are limited^{33,70}. To examine the impact of a single mitotic resetting on loop perturbation, we compared loops dependent on YY1 in asynchronous cells to those dependent on YY1 for establishment in the mitosis-to-G1 transition. Some YY1-YY1 loops that required YY1 selectively for their establishment following mitosis were maintained without YY1 in asynchronous cells (Fig. 7a–c). These differences were partly attributable to loops that were present in synchronized G1 cells but weaker in asynchronous cells (Fig. 7d and Extended Data Fig. 7j,k).

Certain genes also relied on YY1 for re-activation after mitosis yet could maintain transcriptional output in the absence of YY1 in asynchronous cells (Fig. 7e,f). Genes that were solely dependent on YY1 during re-activation were significantly enriched in CRE loops exclusively reliant on YY1 for establishment after mitosis (Fig. 7g). Thus, the requirements for YY1 binding can differ for loop establishment following mitosis and loop maintenance in interphase. Moreover, YY1-dependent looping potentially regulates transcription in a cell cycle stage-specific manner. Assays of asynchronous cells may miss YY1-dependent loops that are strong, and perhaps functionally significant, at specific timepoints but concealed when averaging across populations.

Discussion

Effects of acute transcription factor depletion on CRE looping have been underexplored, especially in the context of loop establishment

during the mitosis-to-G1 transition. Through acute YY1 depletion—in asynchronous cells and synchronized cells exiting mitosis—we have identified an immediate requirement for YY1 in chromatin looping and transcription. Moreover, our results argue against a CTCF-like mechanism in which YY1 functions as a cohesin loop extrusion blocker. However, depending on context, the process of loop extrusion may facilitate encounters between YY1-bound CREs.

YY1 loss-induced loop changes occurred even in the absence of differences in H3K27ac and LDB1 ChIP-seq chromatin occupancy peaks, suggesting that YY1's activity cannot simply be attributed to perturbation of enhancer activity. We speculate that the dimerization of YY1 (refs. 43,48,50,60,61) may contribute to its looping mechanism. However, cases in which YY1 binding at loop anchors is uncoupled from looping suggest that YY1 is dispensable for a subset of loops and, conversely, insufficient to form loops on its own.

Chromatin looping and transcription appeared to be uncorrelated in the majority of cases with the following caveats: (1) short-range loops, which tend to be independent of cohesin, are missed due to resolution limits; (2) YY1-dependent promoters frequently engage in additional, YY1-independent loops, linking them to enhancer elements that may compensate for the lost enhancer contacts and (3) looping and transcription may not be directly coupled on a chronological scale. For example, during gene activation in G1, additional postlooping events may be limiting. In the case of YY1 depletion in asynchronously growing cells, loops may be maintained by factors other than YY1. Hence, we believe that we may be underestimating the correlation between YY1-dependent looping and YY1-dependent transcription. The link between transcription and looping is also confounded by the ways differential loops are quantified. We compared multiple tools (that is, cooltools⁷⁷, Mustache¹⁰⁹ and Chromosight¹¹⁰), which revealed that the choice of algorithm and associated parameters can markedly affect the number of differential loops called. Therefore, in general, clear

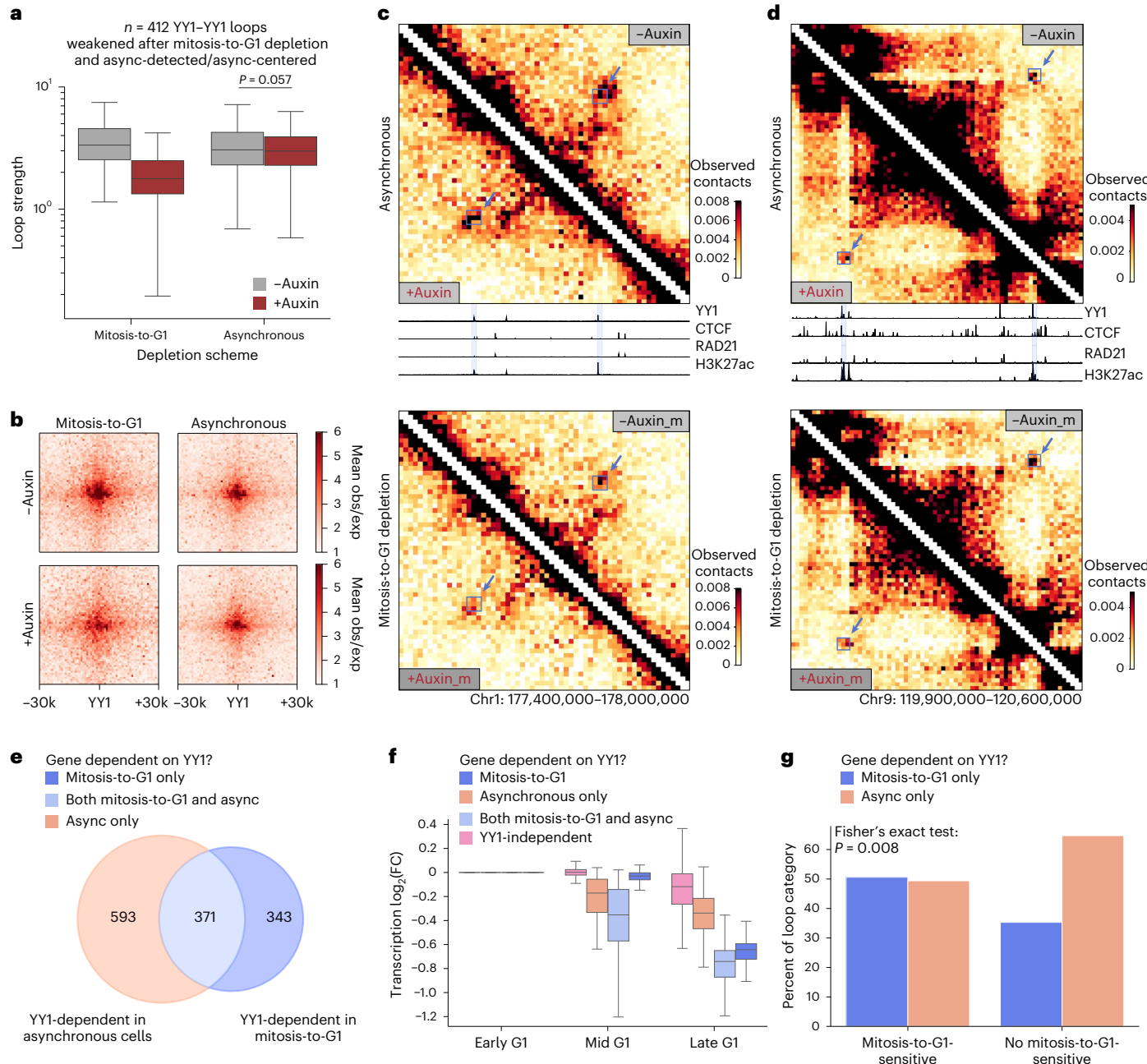


Fig. 7 | Cell-cycle-dependent YY1 requirements for CRE loop formation. **a**, Box plot showing loop strengths of YY1-YY1 loops weakened by mitosis-to-G1 depletion of YY1 (two-sided Mann-Whitney *U* test). Only loops called in both mid G1 and asynchronous cells are included. Loop coordinates from asynchronous cells were used in instances where loop centers were adjacent but not identical. **b**, Pileup plots corresponding to loops included in **a**. **c**, **d**, Example of a loop insensitive to YY1 depletion in asynchronous cells (top) but sensitive to mitosis-to-G1 depletion (bottom). ChIP-seq tracks from asynchronous YY1-AID cells are shown. The same loop is highlighted in Fig. **5d**. **e**, Another example

of a loop that is more sensitive to mitosis-to-G1 depletion. **e**, Venn diagram of genes downregulated after YY1 depletion in asynchronous cells and genes downregulated after YY1 depletion in the mitosis-to-G1 transition. **f**, Box plot showing $\log_2(+\text{auxin}/-\text{auxin})$ transcriptional change at different G1 stages. Genes are stratified based on the depletion scheme in which they were YY1-dependent. **g**, Bar plot showing the percentage of genes that overlap with a CRE loop weakened only in the mitosis-to-G1 interval. Genes are stratified based on the depletion scheme in which they were YY1-dependent.

parameter descriptions and additional benchmarking are needed to quantify loop changes and to enable comparisons between studies.

Several lines of evidence suggest that YY1 forms loops without direct reliance on the CTCF-cohesin machinery or cohesin blocking: 1) YY1-dependent CRE loop anchors tend to be less occupied by CTCF-cohesin, 2) chromatin occupancy of CTCF-cohesin is robust to YY1 depletion, and 3) YY1-dependent focal contacts are preserved upon CTCF-cohesin depletion. Surprisingly, a subset of structural loops was

affected by YY1 loss, although the effects were more focal compared to changes upon CTCF or cohesin depletion. The reason for changes to structural loops and YY1-unoccupied loops remains unclear. We speculate that the loss of a YY1-bound loop could collaterally affect nested or encompassing YY1-unoccupied loops with nearby loop anchors.

Consistent with past studies^{16–21,111}, cohesin depletion variably affected CRE contacts, including those dependent on YY1. Despite cohesin loss, certain YY1-bound loop anchors can still form punctate

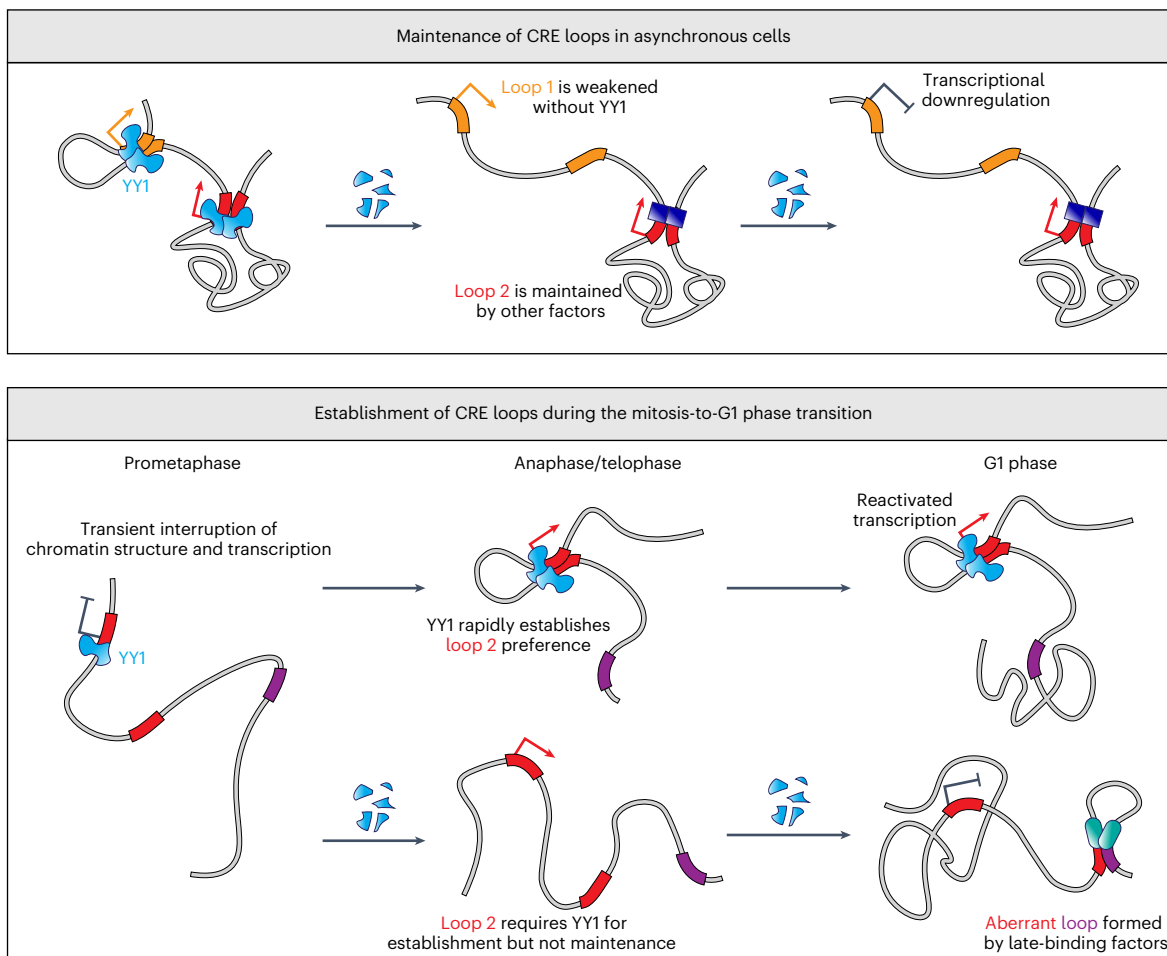


Fig. 8 | Model for CRE loop establishment and maintenance following mitosis.

In asynchronous cells (top), certain CRE loops are sensitive to YY1 depletion (for example, loop 1), while others can be maintained by other factors besides YY1 (for example, loop 2). Transcriptional downregulation can occur due to the loss of a CRE loop. In the mitosis-to-G1 transition (bottom), YY1 binding rapidly establishes the specificity of CRE pairing in anaphase/telophase and initiates transcription in G1. When YY1 is depleted throughout the mitosis-to-G1

transition, YY1-dependent CRE loops fail to establish, subsequently enabling late-binding factors to form aberrant loops. For certain loops (for example, loop 2), YY1 is required to establish looping and transcription after mitosis but is dispensable for their maintenance in interphase. Loops can dynamically form and dissolve within each stage, so the illustration of maintained loops represents the preserved frequency of looping rather than a stable structure across multiple timepoints.

contacts. Perhaps the minimal transcription perturbations reported after cohesin depletion^{16–20,112} are partly due to the preservation of loop strength (that is, contacts relative to local background) despite the global dampening of long-range interactions.

We also uncovered differences between YY1 requirements for the maintenance versus the establishment of chromatin looping. This aligns with previous observations that the formation of certain chromatin structures requires passage through mitosis^{25,102–104}. We propose a model in which early binding factors such as YY1 may establish the specificity of E-P pairing in anaphase/telophase but become dispensable in G1 if additional late-binding factors maintain loop specificity (Fig. 8). This model could explain why some YY1-bound loops are resistant to depletion in asynchronous cells.

In sum, we observed that YY1 is acutely necessary for both the establishment and maintenance of a subset of chromatin loops through a cohesin-independent mechanism. Given the limited number of acute degron-based studies of CRE-binding factors, it remains to be seen how the effects of YY1 depletion compare to those of other transcription factors. CRE loops, unlike CTCF-cohesin-mediated structural loops, may be formed and maintained by diverse combinations of factors, limiting the effect sizes that can be observed within a single perturbation scheme. Future studies of multiple CRE-binding factors within

the same cell type could help support a model where the multiplicity of looping factors enables specificity and precision in E-P pairing across space and time.

Online content

Any methods, additional references, Nature Portfolio reporting summaries, source data, extended data, supplementary information, acknowledgements, peer review information; details of author contributions and competing interests; and statements of data and code availability are available at <https://doi.org/10.1038/s41588-024-01871-y>.

References

1. Furlong, E. E. M. & Levine, M. Developmental enhancers and chromosome topology. *Science* **361**, 1341–1345 (2018).
2. Zheng, H. & Xie, W. The role of 3D genome organization in development and cell differentiation. *Nat. Rev. Mol. Cell Biol.* **20**, 535–550 (2019).
3. Zhang, H. & Blobel, G. A. Genome folding dynamics during the M-to-G1-phase transition. *Curr. Opin. Genet Dev.* **80**, 102036 (2023).
4. Fudenberg, G. et al. Formation of chromosomal domains by loop extrusion. *Cell Rep.* **15**, 2038–2049 (2016).

5. Davidson, I. F. et al. DNA loop extrusion by human cohesin. *Science* **366**, 1338–1345 (2019).
6. Kim, Y., Shi, Z., Zhang, H., Finkelstein, I. J. & Yu, H. Human cohesin compacts DNA by loop extrusion. *Science* **366**, 1345–1349 (2019).
7. de Wit, E. et al. CTCF binding polarity determines chromatin looping. *Mol. Cell* **60**, 676–684 (2015).
8. Guo, Y. et al. CRISPR inversion of CTCF sites alters genome topology and enhancer/promoter function. *Cell* **162**, 900–910 (2015).
9. Rao, S. S. P. et al. A 3D map of the human genome at kilobase resolution reveals principles of chromatin looping. *Cell* **159**, 1665–1680 (2014).
10. Sanborn, A. L. et al. Chromatin extrusion explains key features of loop and domain formation in wild-type and engineered genomes. *Proc. Natl Acad. Sci. USA* **112**, E6456–E6465 (2015).
11. Davidson, I. F. & Peters, J.-M. Genome folding through loop extrusion by SMC complexes. *Nat. Rev. Mol. Cell. Biol.* **22**, 445–464 (2021).
12. Alipour, E. & Marko, J. F. Self-organization of domain structures by DNA-loop-extruding enzymes. *Nucleic Acids Res.* **40**, 11202–11212 (2012).
13. Nasmyth, K. Disseminating the genome: joining, resolving, and separating sister chromatids during mitosis and meiosis. *Annu. Rev. Genet.* **35**, 673–745 (2001).
14. Riggs, A. D. DNA methylation and late replication probably aid cell memory, and type I DNA reeling could aid chromosome folding and enhancer function. *Philos. Trans. R. Soc. Lond. B Biol. Sci.* **326**, 285–297 (1990).
15. de Wit, E. & Nora, E. P. New insights into genome folding by loop extrusion from inducible degron technologies. *Nat. Rev. Genet.* **24**, 73–85 (2023).
16. Rhodes, J. D. P. et al. Cohesin disrupts polycomb-dependent chromosome interactions in embryonic stem cells. *Cell Rep.* **30**, 820–835 (2020).
17. Kriz, A. J., Colognori, D., Sunwoo, H., Nabet, B. & Lee, J. T. Balancing cohesin eviction and retention prevents aberrant chromosomal interactions, polycomb-mediated repression, and X-inactivation. *Mol. Cell* **81**, 1970–1987 (2021).
18. Rao, S. S. P. et al. Cohesin loss eliminates all loop domains. *Cell* **171**, 305–320 (2017).
19. Hsieh, T.-H. S. et al. Enhancer–promoter interactions and transcription are largely maintained upon acute loss of CTCF, cohesin, WAPL or YY1. *Nat. Genet.* **54**, 1919–1932 (2022).
20. Thiecke, M. J. et al. Cohesin-dependent and -independent mechanisms mediate chromosomal contacts between promoters and enhancers. *Cell Rep.* **32**, 107929 (2020).
21. Wutz, G. et al. Topologically associating domains and chromatin loops depend on cohesin and are regulated by CTCF, WAPL, and PDS5 proteins. *EMBO J.* **36**, 3573–3599 (2017).
22. Khatabi, L. E. et al. A pliable mediator acts as a functional rather than an architectural bridge between promoters and enhancers. *Cell* **178**, 1145–1158 (2019).
23. Goel, V.Y., Huseyin, M.K. & Hansen, A. S. Region Capture Micro-C reveals coalescence of enhancers and promoters into nested microcompartments. *Nat. Genet.* **55**, 1048–1056 (2023).
24. Zhang, H. et al. CTCF and transcription influence chromatin structure re-configuration after mitosis. *Nat. Commun.* **12**, 5157 (2021).
25. Nora, E. P. et al. Targeted degradation of CTCF decouples local insulation of chromosome domains from genomic compartmentalization. *Cell* **169**, 930–944 (2017).
26. Li, X. et al. GAGA-associated factor fosters loop formation in the *Drosophila* genome. *Mol. Cell* **83**, 1519–1526 (2023).
27. Linares-Saldana, R. et al. BRD4 orchestrates genome folding to promote neural crest differentiation. *Nat. Genet.* **53**, 1480–1492 (2021).
28. Crump, N. T. et al. BET inhibition disrupts transcription but retains enhancer–promoter contact. *Nat. Commun.* **12**, 223 (2021).
29. Jaeger, M. G. et al. Selective mediator dependence of cell-type-specifying transcription. *Nat. Genet.* **52**, 719–727 (2020).
30. Sun, F. et al. The Pol II preinitiation complex (PIC) influences mediator binding but not promoter–enhancer looping. *Gene Dev.* **35**, 1175–1189 (2021).
31. Ramasamy, S. et al. The mediator complex regulates enhancer–promoter interactions. *Nat. Struct. Mol. Biol.* **30**, 991–1000 (2023).
32. Kagey, M. H. et al. Mediator and cohesin connect gene expression and chromatin architecture. *Nature* **467**, 430–435 (2010).
33. Zhang, S. et al. RNA polymerase II is required for spatial chromatin reorganization following exit from mitosis. *Sci. Adv.* **7**, eabg8205 (2021).
34. Zhang, S., Übelmessier, N., Barbieri, M. & Papantonis, A. Enhancer–promoter contact formation requires RNAPII and antagonizes loop extrusion. *Nat. Genet.* **55**, 832–840 (2023).
35. Jiang, Y. et al. Genome-wide analyses of chromatin interactions after the loss of Pol I, Pol II, and Pol III. *Genome Biol.* **21**, 158 (2020).
36. Hsieh, T.-H. S. et al. Resolving the 3D landscape of transcription-linked mammalian chromatin folding. *Mol. Cell* **78**, 539–553 (2020).
37. Barshad, G. et al. RNA polymerase II dynamics shape enhancer–promoter interactions. *Nat. Genet.* **55**, 1370–1380 (2023).
38. Hwang, S. S. et al. Transcription factor YY1 is essential for regulation of the Th2 cytokine locus and for Th2 cell differentiation. *Proc. Natl Acad. Sci. USA* **110**, 276–281 (2013).
39. Beagan, J. A. et al. YY1 and CTCF orchestrate a 3D chromatin looping switch during early neural lineage commitment. *Genome Res.* **27**, 1139–1152 (2017).
40. Liu, H. et al. Yin Yang 1 is a critical regulator of B-cell development. *Gene Dev.* **21**, 1179–1189 (2007).
41. Degner, S. C. et al. CCCTC-binding factor (CTCF) and cohesin influence the genomic architecture of the IgH locus and antisense transcription in pro-B cells. *Proc. Natl Acad. Sci. USA* **108**, 9566–9571 (2011).
42. Verma-Gaur, J. et al. Noncoding transcription within the IgH distal VH region at PAIR elements affects the 3D structure of the IgH locus in pro-B cells. *Proc. Natl Acad. Sci. USA* **109**, 17004–17009 (2012).
43. Mehra, P. et al. YY1 controls Eμ-3'RR DNA loop formation and immunoglobulin heavy chain class switch recombination. *Blood Adv.* **1**, 15–20 (2016).
44. Perreault, A. A., Brown, J. D. & Venters, B. J. Erythropoietin regulates transcription and YY1 dynamics in a pre-established chromatin architecture. *iScience* **23**, 101583 (2020).
45. Fang, S. et al. Tet inactivation disrupts YY1 binding and long-range chromatin interactions during embryonic heart development. *Nat. Commun.* **10**, 4297 (2019).
46. Kwon, D. Y. et al. Neuronal Yin Yang1 in the prefrontal cortex regulates transcriptional and behavioral responses to chronic stress in mice. *Nat. Commun.* **13**, 55 (2022).
47. Atlasi, Y. et al. Epigenetic modulation of a hardwired 3D chromatin landscape in two naive states of pluripotency. *Nat. Cell Biol.* **21**, 568–578 (2019).
48. Li, L. et al. YY1 interacts with guanine quadruplexes to regulate DNA looping and gene expression. *Nat. Chem. Biol.* **17**, 161–168 (2021).
49. Liu, T. et al. Matrin3 mediates differentiation through stabilizing chromatin loop-domain interactions and YY1 mediated enhancer–promoter interactions. *Nat. Commun.* **15**, 1274 (2024).
50. Weintraub, A. S. et al. YY1 is a structural regulator of enhancer–promoter loops. *Cell* **171**, 1573–1588 (2017).

51. Cubeñas-Potts, C. & Corces, V. G. Architectural proteins, transcription, and the three-dimensional organization of the genome. *FEBS Lett.* **589**, 2923–2930 (2015).
52. Kim, S. & Shendure, J. Mechanisms of interplay between transcription factors and the 3D genome. *Mol. Cell* **76**, 306–319 (2019).
53. Lee, J., Krivega, I., Dale, R. K. & Dean, A. The LDB1 complex co-opts CTCF for erythroid lineage-specific long-range enhancer interactions. *Cell Rep.* **19**, 2490–2502 (2017).
54. Monahan, K., Horta, A. & Lomvardas, S. LHX2- and LDB1-mediated trans interactions regulate olfactory receptor choice. *Nature* **565**, 448–453 (2019).
55. Krivega, I. & Dean, A. LDB1-mediated enhancer looping can be established independent of mediator and cohesin. *Nucleic Acids Res.* **45**, 8255–8268 (2017).
56. Deng, W. et al. Controlling long-range genomic interactions at a native locus by targeted tethering of a looping factor. *Cell* **149**, 1233–1244 (2012).
57. Deng, W. et al. Reactivation of developmentally silenced globin genes by forced chromatin looping. *Cell* **158**, 849–860 (2014).
58. Vakoc, C. R. et al. Proximity among distant regulatory elements at the β -globin locus requires GATA-1 and FOG-1. *Mol. Cell* **17**, 453–462 (2005).
59. Breda, L. et al. Forced chromatin looping raises fetal hemoglobin in adult sickle cells to higher levels than pharmacologic inducers. *Blood* **128**, 1139–1143 (2016).
60. López-Perrote, A. et al. Structure of Yin Yang 1 oligomers that cooperate with RuvBL1–RuvBL2 ATPases. *J. Biol. Chem.* **289**, 22614–22629 (2014).
61. Wu, S. et al. A YY1–INO80 complex regulates genomic stability through homologous recombination-based repair. *Nat. Struct. Mol. Biol.* **14**, 1165–1172 (2007).
62. Lu, Z., Assumpção, A. L. F. V., Viny, A. D., Levine, R. L. & Pan, X. YY1 controls hematopoietic stem cell quiescence by repressing cohesin expression. *Blood* **132**, 3831 (2018).
63. Pan, X. et al. YY1 controls Igk repertoire and B-cell development, and localizes with condensin on the Igk locus. *EMBO J.* **32**, 1168–1182 (2013).
64. Donohoe, M. E., Zhang, L.-F., Xu, N., Shi, Y. & Lee, J. T. Identification of a Ctcf cofactor, Yy1, for the X chromosome binary switch. *Mol. Cell* **25**, 43–56 (2007).
65. Pentland, I. et al. Disruption of CTCF-YY1-dependent looping of the human papillomavirus genome activates differentiation-induced viral oncogene transcription. *PLoS Biol.* **16**, e2005752 (2018).
66. Guo, C. et al. Two forms of loops generate the chromatin conformation of the immunoglobulin heavy-chain gene locus. *Cell* **147**, 332–343 (2011).
67. Zhang, H. et al. Chromatin structure dynamics during the mitosis-to-G1 phase transition. *Nature* **576**, 158–162 (2019).
68. Naumova, N. et al. Organization of the mitotic chromosome. *Science* **342**, 948–953 (2013).
69. Gibcus, J. H. et al. A pathway for mitotic chromosome formation. *Science* **359**, 6376 (2018).
70. Pelham-Webb, B. et al. H3K27ac bookmarking promotes rapid post-mitotic activation of the pluripotent stem cell program without impacting 3D chromatin reorganization. *Mol. Cell* **81**, 1732–1748 (2021).
71. Abramo, K. et al. A chromosome folding intermediate at the condensin-to-cohesin transition during telophase. *Nat. Cell Biol.* **21**, 1393–1402 (2019).
72. Chervova, A., Festuccia, N., Altamirano-Pacheco, L., Dubois, A. & Navarro, P. A gene subset requires CTCF bookmarking during the fast post-mitotic reactivation of mouse ES cells. *EMBO Rep.* **24**, e56075 (2023).
73. Donohoe, M. E. et al. Targeted disruption of mouse Yin Yang 1 transcription factor results in peri-implantation lethality. *Mol. Cell. Biol.* **19**, 7237–7244 (1999).
74. Coronado, D. et al. A short G1 phase is an intrinsic determinant of naïve embryonic stem cell pluripotency. *Stem Cell Res.* **10**, 118–131 (2013).
75. Weiss, M. J., Yu, C. & Orkin, S. H. Erythroid-cell-specific properties of transcription factor GATA-1 revealed by phenotypic rescue of a gene-targeted cell line. *Mol. Cell. Biol.* **17**, 1642–1651 (1997).
76. Krietenstein, N. et al. Ultrastructural details of mammalian chromosome architecture. *Mol. Cell* **78**, 554–565 (2020).
77. Open2C, et al. Cooltools: enabling high-resolution Hi-C analysis in Python. *PLoS Comput. Biol.* **20**, e1012067 (2024).
78. Zuin, J. et al. Nonlinear control of transcription through enhancer-promoter interactions. *Nature* **604**, 571–577 (2022).
79. Rinzenma, N. J. et al. Building regulatory landscapes reveals that an enhancer can recruit cohesin to create contact domains, engage CTCF sites and activate distant genes. *Nat. Struct. Mol. Biol.* **29**, 563–574 (2022).
80. Xiao, J. Y., Hafner, A. & Boettiger, A. N. How subtle changes in 3D structure can create large changes in transcription. *eLife* **10**, e64320 (2021).
81. Xi, W. & Beer, M. A. Loop competition and extrusion model predicts CTCF interaction specificity. *Nat. Commun.* **12**, 1046 (2021).
82. Schwalie, P. C. et al. Co-binding by YY1 identifies the transcriptionally active, highly conserved set of CTCF-bound regions in primate genomes. *Genome Biol.* **14**, R148 (2013).
83. Lu, Z. et al. Yin Yang 1 regulates cohesin complex protein SMC3 in mouse hematopoietic stem cells. *Blood Adv.* **25**, 3076–3091 (2024).
84. Zhao, H. et al. Genome folding principles uncovered in condensin-depleted mitotic chromosomes. *Nat. Genet.* **56**, 1213–1224 (2024).
85. Calderon, L. et al. Cohesin-dependence of neuronal gene expression relates to chromatin loop length. *eLife* **11**, e76539 (2022).
86. Kane, L. et al. Cohesin is required for long-range enhancer action at the Shh locus. *Nat. Struct. Mol. Biol.* **29**, 891–897 (2022).
87. Shi, Y., Seto, E., Chang, L.-S. & Shenk, T. Transcriptional repression by YY1, a human GLI-Krüppel-related protein, and relief of repression by adenovirus E1A protein. *Cell* **67**, 377–388 (1991).
88. Seto, E., Shi, Y. & Shenk, T. YY1 is an initiator sequence-binding protein that directs and activates transcription in vitro. *Nature* **354**, 241–245 (1991).
89. Park, K. & Atchison, M. L. Isolation of a candidate repressor/activator, NF-E1 (YY-1, δ), that binds to the immunoglobulin kappa 3' enhancer and the immunoglobulin heavy-chain mu E1 site. *Proc. Natl Acad. Sci. USA* **88**, 9804–9808 (1991).
90. Hariharan, N., Kelley, D. E. & Perry, R. P. Delta, a transcription factor that binds to downstream elements in several polymerase II promoters, is a functionally versatile zinc finger protein. *Proc. Natl Acad. Sci. USA* **88**, 9799–9803 (1991).
91. Schwalb, B. et al. TT-seq maps the human transient transcriptome. *Science* **352**, 1225–1228 (2016).
92. Gregersen, L. H., Mitter, R. & Svejstrup, J. Q. Using TTchem-seq for profiling nascent transcription and measuring transcript elongation. *Nat. Protoc.* **15**, 604–627 (2020).
93. Wilkinson, F. H., Park, K. & Atchison, M. L. Polycomb recruitment to DNA in vivo by the YY1 REPO domain. *Proc. Natl Acad. Sci. USA* **103**, 19296–19301 (2006).
94. Shah, M., Funnell, A. P. W., Quinlan, K. G. R. & Crossley, M. Hit and run transcriptional repressors are difficult to catch in the act. *BioEssays* **41**, e1900041 (2019).

95. Banigan, E. J. et al. Transcription shapes 3D chromatin organization by interacting with loop extrusion. *Proc. Natl Acad. Sci. USA* **120**, e2210480120 (2023).
96. Ito, K. & Zaret, K. S. Maintaining transcriptional specificity through mitosis. *Annu. Rev. Genom. Hum. Genet.* **23**, 53–71 (2022).
97. Kadauke, S. & Blobel, G. A. Mitotic bookmarking by transcription factors. *Epigenetics Chromatin* **6**, 6 (2013).
98. Rizkallah, R. & Hurt, M. M. Regulation of the transcription factor YY1 in mitosis through phosphorylation of its DNA-binding domain. *Mol. Biol. Cell* **20**, 4766–4776 (2009).
99. Kassardjian, A. et al. The transcription factor YY1 is a novel substrate for aurora B kinase at G2/M transition of the cell cycle. *PLoS ONE* **7**, e50645 (2012).
100. Alexander, K. E., Rizkallah, R. & Aurora, A. Phosphorylation of YY1 during mitosis inactivates its DNA binding activity. *Sci. Rep.* **7**, 10084 (2017).
101. Hsiung, C. C.-S. et al. Genome accessibility is widely preserved and locally modulated during mitosis. *Genome Res.* **25**, 213–225 (2015).
102. Kumaran, R. I. & Spector, D. L. A genetic locus targeted to the nuclear periphery in living cells maintains its transcriptional competence. *J. Cell Biol.* **180**, 51–65 (2008).
103. Reddy, K. L., Zullo, J. M., Bertolino, E. & Singh, H. Transcriptional repression mediated by repositioning of genes to the nuclear lamina. *Nature* **452**, 243–247 (2008).
104. Bridger, J. M., Boyle, S., Kill, I. R. & Bickmore, W. A. Re-modelling of nuclear architecture in quiescent and senescent human fibroblasts. *Curr. Biol.* **10**, 149–152 (2000).
105. Mach, P. et al. Cohesin and CTCF control the dynamics of chromosome folding. *Nat. Genet.* **54**, 1907–1918 (2022).
106. Chen, H. et al. Dynamic interplay between enhancer–promoter topology and gene activity. *Nat. Genet.* **50**, 1296–1303 (2018).
107. Alexander, J. M. et al. Live-cell imaging reveals enhancer-dependent Sox2 transcription in the absence of enhancer proximity. *eLife* **8**, e41769 (2019).
108. Hsiung, C. C.-S. et al. A hyperactive transcriptional state marks genome reactivation at the mitosis–G1 transition. *Gene Dev.* **30**, 1423–1439 (2016).
109. Arda, A. R., Gezer, H. T., Lonardi, S. & Ay, F. Mustache: multi-scale detection of chromatin loops from Hi-C and Micro-C maps using scale-space representation. *Genome Biol.* **21**, 256 (2020).
110. Matthey-Dore, C. et al. Computer vision for pattern detection in chromosome contact maps. *Nat. Commun.* **11**, 5795 (2020).
111. Vian, L. et al. The energetics and physiological impact of cohesin extrusion. *Cell* **173**, 1165–1178 (2018).
112. Liu, N. Q. et al. WAPL maintains a cohesin loading cycle to preserve cell-type-specific distal gene regulation. *Nat. Genet.* **53**, 100–109 (2021).

Publisher's note Springer Nature remains neutral with regard to jurisdictional claims in published maps and institutional affiliations.

Springer Nature or its licensor (e.g. a society or other partner) holds exclusive rights to this article under a publishing agreement with the author(s) or other rightsholder(s); author self-archiving of the accepted manuscript version of this article is solely governed by the terms of such publishing agreement and applicable law.

© The Author(s), under exclusive licence to Springer Nature America, Inc. 2024

Methods

The experiments mentioned below did not require approval from a specific ethics board.

Cell culture and maintenance

The G1E-ER4 mouse erythroblast line¹¹³ was a gift from M. Weiss. G1E-ER4 cells were cultured in Iscove's Modified Dulbecco's Medium (IMDM) supplemented with 15% FBS, 2% penicillin-streptomycin, Kit ligand, monothioglycerol and erythropoietin. Cells were consistently maintained at a density of less than 1 million cells per ml.

The *Drosophila* Schneider 2 (S2) cell line was purchased from Gibco (R69007). S2 cells were grown at 28 °C in S2 media (Gibco, 21720024) with 0.1% of Pluronic F-68 Nonionic Surfactant (Gibco, 24040032), 10% of fetal bovine serum and penicillin-streptomycin at a final concentration of 50 units penicillin G and 50 µg streptomycin sulfate per ml of media.

Generation of the YY1-AID subline

To degrade endogenous YY1 protein, a mini-AID tag was inserted at both endogenous Yy1 alleles in the G1E-ER4 line. First, a donor template for homology-directed repair was constructed with the following sequences: (1) a 5' homology arm (850 bp) of the sequence upstream of the endogenous Yy1's stop codon, (2) a minimal AID tag (132 bp), (3) a P2A self-cleaving sequence with a GSG linker (66 bp), (4) a mCherry sequence with a stop codon (708 bp) and (5) a 3' homology arm (850 bp) of the sequence downstream of Yy1's stop codon. These sequences were inserted in the abovementioned order in the pUC19 plasmid vector using the Takara In-Fusion HD Cloning Plus Kit (638909). A previously published gRNA sequence⁵⁰ targeting the stop codon of the Yy1 gene was inserted in the px330-GFP (green fluorescent protein) plasmid. Primers and sequences are listed in Supplementary Table 4.

The Amaxa II electroporator (Lonza) and the Amaxa II Cell Line Nucleofector Kit R (Lonza, VCA-1001) were used to transfet G1E-ER4 cells with setting G-016. The transfection reaction consisted of 3 million G1E-ER4 cells, 6 µg of the homology-directed repair template (containing AID-P2A-mCherry) and 18 µg of the px330-GFP construct (containing Cas9 and the gRNA). After transfection, cells were cultured in antibiotic-free media for 28 h. Then, GFP and mCherry double-positive cells were selected via FACS and expanded as single-cell clones. PCR screening followed by Sanger sequencing was used to identify a clone with insertions of AID-P2A-mCherry at both alleles, which will be referred to as the 'YY1-AID' subline hereafter. OsTiR-IRES-GFP was expressed in YY1-AID cells via retroviral vector MigR1. GFP-positive cells were subsequently sorted through FACS.

To validate the expression of the tagged YY1 protein and its responsiveness to auxin induction, Western blot analysis was conducted. YY1-AID cells expressing OsTiR-IRES-GFP were exposed to 1 mM auxin (indole 3-acetic acid sodium salt; Sigma, I5148) for 0, 1, 2 and 4 h. Wild-type G1E-ER4 cells served as a comparison for basal YY1 levels in parental cells. Samples were lysed in complete RIPA (Radio-Immunoprecipitation Assay) lysis buffer, sonicated for 10 min, boiled in Laemmli SDS sample buffer at 95 °C for 5 min and run on a 4–12% Bis-Tris protein gel.

Cell synchronization, auxin treatment and cell sorting

Experiments in asynchronous cells. '+Auxin' YY1-AID cells were treated with 1 mM auxin and collected after 4 h. '-Auxin' YY1-AID cells were cultured under identical conditions without auxin treatment.

YY1 ChIP-seq for mitosis-to-G1 stages. A previously published G1E-ER4 mCherry-MD subline⁶⁷ was used for collecting stage-specific populations for YY1 ChIP-seq. This subline contains a mCherry reporter fused to the cyclin B mitotic degron (MD) domain. Cells at a density of 0.6–0.8 million cells per ml were arrested in prometaphase through treatment of 200 ng ml⁻¹ of nocodazole. After 7 h of nocodazole treatment, prometaphase-enriched cells were collected.

To enrich the remaining mitosis-to-G1 populations, after 7 h of nocodazole treatment, cells were pelleted, washed twice and resuspended in warmed nocodazole-free media. After resuspension, cells were collected at 25 min (for anaphase/telophase), 1 h (for early G1), 2 h (for mid G1) or 4 h (for late G1).

After collection at the abovementioned timepoints, samples were cross-linked with 1% formaldehyde, quenched in 1 M glycine and permeabilized with 0.1% Triton X-100. Cross-linked cells were pelleted at 2,000 rpm for 10 min at 4 °C. For subsequent steps, all buffers were supplemented with 1 mM phenylmethylsulfonyl fluoride (PMSF) and protease inhibitors (Sigma, P8340).

Samples for all timepoints were stained with anti-pMPM2 antibody (Millipore, 05-368) at a concentration of 0.5 µl per 10 million cells for 50 min at room temperature and then stained with Allophycocyanin (APC)-conjugated F(ab')2-Goat anti-Mouse secondary antibody (Thermo Fisher Scientific, 17-4010-82) at a concentration of 2 µl per 10 million cells for 30 min at room temperature in dark. Cells were resuspended in FACS-sorting buffer containing 25 ng ml⁻¹ DAPI and kept on ice.

FACS on the MoFlo Astrios EQ sorter (Beckman Coulter) was used to purify stage-specific populations. Prometaphase samples were sorted based on positive pMPM2, positive mCherry-MD and 4N DAPI signals. Anaphase/telophase samples were sorted based on reduced mCherry-MD and 4N DAPI signals. Early G1, mid G1 and late G1 samples were sorted based on negative mCherry-MD and 2N DAPI signals. Cells were kept at 4 °C for the duration of the sort. Representative FACS plots are shown in Extended Data Fig. 6a.

Synchronization of YY1-AID cells. Control –auxin and treated +auxin samples were cultured and treated identically, other than the auxin treatment itself. YY1-AID cells were treated with 200 ng ml⁻¹ nocodazole for 7 h. In the final 4 h of nocodazole treatment, 1 mM auxin was added to the +auxin sample. In this manner, at the start of release from prometaphase, +auxin samples would have been treated with auxin for 4 h, an amount of time sufficient for YY1 degradation. To enrich for G1 populations, after 7 h of nocodazole treatment, cells were pelleted, washed twice and resuspended in warmed nocodazole-free media (\pm 1 mM auxin).

Synchronized YY1-AID samples used in ChIP-seq. After resuspension, cells were collected at 1 h (for early G1), 2 h (for mid G1) or 4 h (for late G1). After collection at the abovementioned timepoints, samples were cross-linked with 1% formaldehyde for 10 min, quenched in 1 M glycine and permeabilized with 0.1% Triton X-100. Cross-linked cells were pelleted at 2,000 rpm for 10 min at 4 °C. For subsequent steps, all buffers were supplemented with PMSF and protease inhibitors. Cells were resuspended in FACS-sorting buffer containing 25 ng ml⁻¹ DAPI and kept on ice. G1 populations were sorted using the gating strategy described above.

Synchronized YY1-AID samples used for Micro-C. Cells were subjected to 7 h of nocodazole treatment (\pm 4 h auxin treatment) and 2 h of release in nocodazole-free media \pm auxin. After collection, samples were cross-linked at room temperature with 1% formaldehyde for 10 min and quenched in 125 mM glycine. Cells were then cross-linked in 3 mM disuccinimidyl glutarate (DSC; Thermo Fisher Scientific, 20593) at room temperature for 40 min and quenched with 0.4 M glycine. Cells were permeabilized with 0.1% Triton X-100, resuspended in FACS-sorting buffer containing 25 ng ml⁻¹ DAPI and kept on ice. Mid G1 samples were sorted as described above.

Generation of ChIP-seq libraries

The following antibodies were used for ChIP: Pol II (Rpb1 NTD (D8L4Y) Rabbit mAb Cell Signaling 14958), YY1 (Active Motif, 61779), RAD21 (Abcam, ab992), CTCF (Millipore, 07-729), LDB1 (anti-CLIM2; Santa Cruz Biotechnology, sc-365074) and H3K27ac (Active Motif, 39133).

Cells were cross-linked with 1% formaldehyde (with 2 mM EDTA) for 10 min and quenched with 1 M glycine for 5 min. Subsequent steps until the elution step were performed at 4 °C. All ChIP buffers were supplemented with protease inhibitors and 1 mM PMSF.

Cell pellets of 10 million cells were incubated in cell lysis buffer (10 mM Tris (pH 8), 0.2% Igepal and 10 mM NaCl) on ice for 20 min. For prometaphase (4 N) and anaphase/telophase (4 N) samples, 5 million cells were used to match the DNA content of other samples (2 N).

Nuclei were pelleted and incubated in nuclei lysis buffer (50 mM Tris (pH 8), 1% SDS and 10 mM EDTA) for 20 min. Samples were sonicated for 5 min (30 s on, 30 s off, ‘easy’ mode) with the Bioruptor Pico (Diagenode). Nuclear extracts were then precleared with 50 µg isotype-matched IgG and 50 µl A/G agarose beads overnight. From the precleared chromatin, 200 µl was set aside as input, while 4.4 ml was used for immunoprecipitation. Antibody-bound A/G agarose beads were incubated with chromatin overnight. Afterwards, beads were washed with IP (immunoprecipitation) wash buffer 1 (20 mM Tris (pH 8), 2 mM EDTA, 50 mM NaCl, 1% Triton X-100 and 0.1% SDS), twice with high salt buffer (20 mM Tris (pH 8), 2 mM EDTA, 500 mM NaCl, 1% Triton X-100 and 0.01% SDS), IP wash buffer 2 (10 mM Tris (pH 8), 1 mM EDTA, 0.25 M LiCl, 1% Igepal and 1% sodium deoxycholate) and twice with TE (10 mM Tris (pH 8) and 1 mM EDTA (pH 8)). At this point, samples were moved to room temperature and DNA was eluted from beads with 200 µl elution buffer (100 mM NaHCO₃ and 1% SDS). Inputs and samples were incubated at 37 °C for 30 min after the addition of 2 µl of 5 M NaCl and 2 ml RNaseA (10 mg ml⁻¹; Roche, 10109169001). In total, 3 µl of proteinase K (20 mg ml⁻¹; BMB, 3115879) was added, and inputs and samples were incubated overnight at 65 °C. In total, 10 µl of 3 M sodium acetate (pH 5) was added, and DNA purification was performed using the QIAquick PCR Purification kit (Qiagen, 28106).

ChIP-qPCR was performed using the Power SYBR Green PCR Master Mix (Thermo Fisher Scientific, 4367660) on an ABI Vii7 real-time PCR machine (primer sequences are listed in Supplementary Table 4).

For ChIP-seq, library preparation was performed with the NEBNext Ultra II DNA Library Prep Kit for Illumina (New England Biolabs (NEB), E7635) using unique dual-indexed primers (NEB, E6440). Paired-end 2× 50 bp sequencing data were generated on the NextSeq 500 or NextSeq 2000 (Illumina). Fastq files were generated with Bclfastq2 v2.15.04 (default parameters). For each experimental condition and subline, a matched input sample was also sequenced, except in cases where sequencing for a matched input was previously published.

Generation of Micro-C libraries

Micro-C was performed as described in a published protocol⁷⁶ with minor adjustments detailed below. Briefly, each biological replicate (10 million cells) was split into two Micro-C reactions with 5 million cells each. The two Micro-C samples for each biological replicate were pooled together again before library preparation.

Samples were cross-linked at room temperature with 1% formaldehyde for 10 min and quenched in 125 mM glycine. Cells were then cross-linked in 3 mM DSG at room temperature for 40 min, quenched with 0.4 M glycine and pelleted.

Cells were lysed and permeabilized in MB 1 (50 mM NaCl, 10 mM Tris-HCl, 5 mM MgCl₂, 1 mM CaCl₂, 0.2% NP-40 and proteinase inhibitor) at 1 million cells per 100 µl for 20 min on ice. Nuclei were pelleted, resuspended in MB 1 and treated with 10 U MNase (Worthington Biochemical, LS004797) for 10 min at 37 °C. MNase was titrated such that chromatin was digested to a 9:1 monomer:dimer ratio. EGTA (egta-zinc acid) was added to a final concentration of 4 mM to stop digestion. Fragments were dephosphorylated with 5 Ur-SAP (NEB, M0371S) for 45 min at 37 °C in dephosphorylation buffer (50 mM NaCl, 10 mM Tris-HCl, 10 mM MgCl₂ and 100 µg ml⁻¹BSA) and then end-chewed with 20 UT4 PNK (NEB, M0201L) and 40 U large Klenow Fragment (NEB, M0210L) for 15 min at 37 °C in 50 mM NaCl, 10 mM Tris-HCl, 10 mM MgCl₂,

100 µg ml⁻¹ BSA, 2 mM ATP and 3 mM DTT. For end-labeling, samples were incubated with biotin-dATP (Jena Biosciences, NU-835-BIO14-S), biotin-dCTP (Jena Biosciences, NU-809-BIOX-S), dTTP and dGTP for 45 min at 25 °C. Proximity ligation was performed using 15,000 U of T4 DNA ligase (NEB, M0202L) at room temperature for 3 h in a total of 2.5 ml of 1× T4 DNA ligase buffer with ATP (NEB, B0202S). Samples were resuspended in 200 µl 1× NEBuffer1 (B7001S), and 200 U of exonuclease III (NEB, M0206S) was added for 10 min at 37 °C to remove unligated ends. For reverse cross-linking, samples were incubated with 25 µl proteinase K (20 mg ml⁻¹), 25 µl 10% SDS and 1.5 µl RNase (10 mg ml⁻¹) overnight at 65 °C.

DNA was purified using phenol:chloroform:isoamyl alcohol extraction and ethanol precipitation. Gel extraction was used to select fragments between 250 and 400 bp. DNA was purified with a Zymoclean Gel DNA Recovery Kit (D4007) and eluted in 50 µl elution buffer. At this point, the two reactions for a given biological replicate were pooled together.

On-bead library preparation was performed with MyONE Streptavidin C1 Dynabeads (Invitrogen, 65001) using the NEBNext Ultra II DNA Library Prep Kit (NEB, E7635) and unique dual-indexed primers (NEB, E6440). Library amplification was performed with the KAPA HiFi Hot Start Mix (KAPA, KK2601). Paired-end 2× 50 bp sequencing data were generated on the NextSeq 500 or NextSeq 2000 (Illumina). Fastq files were generated with Bclfastq2 v2.15.04 (default parameters).

Quantification and data analysis

ChIP-seq preprocessing, peak calling and quantification. Two to three biological replicates of ChIP-seq experiments were performed for each cell line, factor and condition. Analysis scripts have been deposited in Zenodo¹¹⁴. ChIP input material corresponding to each cell line and treatment condition was also sequenced. For each replicate, we aligned reads to the mm9 reference genome using bowtie2 (v2.2.5)^{115,116}. We filtered out duplicate reads and reads with mapping quality (MAPQ) <20 using SAMtools (v1.14)¹¹⁷. We generated a bigwig file of RPM (reads per million) values for each replicate using deeptools (v3.5.1) bamCoverage (binSize = 20, smoothLength = 60, normalizeUsing = BPM). To generate summary bigwigs, we used deeptools bamCompare to average RPM-normalized values across replicates. We used deeptools plotHeatmap to generate heatmaps and profiles of ChIP-seq signals.

We called narrow peaks for each replicate using macs2 (v2.2.7)¹¹⁸ callpeak with the paired-end setting and a matched input file. The peak-calling threshold was set to $q = 0.05$. We combined peaks from each replicate using DiffBind (v3.5)¹¹⁹, which recentered and trimmed peaks to standardized 400 bp intervals based on read enrichment. Peaks located in mm9 blacklist regions from ENCODE were filtered out.

For YY1, to create a list of high-confidence peaks, we only kept peaks that were present in at least two biological replicates. We made one consensus peak list for asynchronous YY1-AID cells and a separate consensus peak list for mitosis-to-G1 sorted cells. In the mitosis-to-G1 YY1 ChIP-seq series, the ‘time of YY1 detection’ was defined as the earliest timepoint at which a YY1 peak was called in any replicate.

For all other factors, we created a consensus list of peaks by taking the union of all peaks across conditions. For H3K27ac peaks, we merged any peaks that were closer than 1 kbp using pybedtools (0.8.2)^{120,121}. Analysis of peak overlap between factors was also performed with pybedtools.

DiffBind was used to quantify transcription factor binding at consensus peaks. Unnormalized read counts were used as input for DESeq2 (v1.32.0)¹²² to identify differentially bound regions based on a significance cutoff of $P_{adj} < 0.05$.

We used the findMotifsGenome.pl script from HOMER¹²³ software suite to identify a YY1 consensus motif enriched in mitosis-to-G1 YY1 ChIP-seq peaks. The scanMotifGenomewide.pl was then used to identify locations of YY1 motifs genome wide.

For Pol II ChIP-seq, deeptools¹²⁴, multiBamSummary was used to quantify reads over the gene body, defined as 750 bp upstream of the transcription start site (TSS) to 1,500 bp downstream of the transcription end site of the longest transcript for each gene. Unnormalized read counts were used as input for DESeq2 to identify differentially bound gene bodies. After analysis with DESeq2, differentially bound genes were additionally filtered to only include genes with an active promoter, defined by direct overlap with both H3K27ac and Pol II peaks. In mitosis-to-G1 experiments, the expression of each gene can vary with timepoint in untreated cells, breaking the biological assumptions of DESeq2 differential analysis, which assumes most genes have similar expression levels across all samples. Thus, we conducted a separate normalization and differential analysis for each timepoint to compare –auxin and +auxin expression. One biological replicate of late G1 untreated YY1–AID was excluded from analysis due to low signal and detection as an outlier in principal component analysis. We used a significance threshold of Benjamini–Hochberg corrected $P_{adj} < 0.05$. The apglm method was used to shrink log(fold change) values¹²⁵.

Generating and visualizing Micro-C contact maps. The distiller pipeline v3.3 (<https://github.com/mirnylab/distiller-nf>) was used to generate contact maps from fastq sequencing files. A balanced contact map was generated for each condition by merging biological replicates after removing PCR duplicates from each replicate. Default settings were used for iterative correction and eigenvector decomposition (ICE) balancing. log-binned contact decay curves (a.k.a. $P(s)$ curves) were generated for contact maps from each biological replicate using cooltools v0.5.1 (ref. 77; <https://github.com/mirnylab/cooltools>).

Coolbox (v0.3.8)¹²⁶ was used for the visualization of contact maps and corresponding ChIP-seq tracks. Unless otherwise stated, all contact map color scales correspond to the observed, ICE-normalized contacts.

For pileup plots of Micro-C contact maps, the software cooltools was used to average signal across all loop regions. In the case of 1 kbp resolution pileups, loop coordinates were refined to be centered on the strongest YY1 peak (or H3K27ac peak) within each loop anchor.

Loop calling and quantification. We used the cooltools.dots function to identify loops in each merged contact map in asynchronous cells. This program implements an approach similar to the published HIC-CUPS algorithm⁹. For each condition, we first called loops on 5 kbp and 10 kbp resolution maps separately. We used the following parameters: max_loci_separation = 2,000,000 (that is, maximum loop length of 2 Mb), clustering_radius = 20,000 (that is, merging of dots that are within 20 kb), lambda_bin_fdr = 0.05 (that is, false discovery rate (FDR) of 0.05) and n_lambda_bins = 50.

We used default settings for defining ‘dots’ that were enriched relative to the following four local neighborhoods: ‘donut’ ($w = 5, P = 2$), ‘vertical’, ‘horizontal’ and ‘lowleft’, except we made the ‘donut’ and ‘lowleft’ neighborhoods rounded, as depicted in the cooltools documentation (<https://cooltools.readthedocs.io/en/latest/notebooks/dots.html>). Default enrichment thresholds were used to minimize false-positive loop calls—loops had to be 1.5-fold enriched over both ‘vertical’ and ‘horizontal’ neighborhoods, 1.75-fold enriched over both ‘donut’ and ‘lower left’ neighborhoods and 2-fold enriched over either the ‘donut’ and ‘lower left’ neighborhoods. Any loop that was a single enriched pixel, rather than a cluster of enriched pixels, was subject to the stricter FDR threshold of 0.02.

After generating 5k and 10k loop lists for –auxin and +auxin samples, we merged loops across all lists. For merging, loops were considered redundant if they were the same pixel or adjacent pixels. We first merged 10k –auxin and 10k +auxin loops that were redundant. We kept the –auxin coordinates in situations where the –auxin and +auxin peaks were in adjacent but nonidentical pixels. Then we merged 5k –auxin and 5k +auxin loops that were redundant. Then we merged these 5k and

10k loop lists, keeping the 5k loop in cases where a loop was detected in both resolutions. This resulted in a combined loop list containing nonoverlapping loops across –auxin and +auxin conditions at either 5k or 10k resolutions. One loop was removed from the list after being manually identified as an artifact.

We quantified loop strength as an observed over locally adjusted expected value. This approach considers the enrichment of a loop relative to its local ‘donut’ neighborhood. For a given loop’s peak pixel, the observed value was first calculated at the resolution at which the loop was called. A locally adjusted expected value was then calculated by multiplying the global expected value at the loop’s peak pixel by a local adjustment value (that is, the sum of the observed contacts within the rounded donut region divided by the sum of the expected contacts within the rounded donut). For each loop, loop strength was calculated in both –auxin and +auxin conditions. Loops with calculated strength of 0, NA or infinite values were filtered out to remove loops in sparse areas that did not consistently show adequate coverage across conditions.

Visual inspection of loop calls showed that simple binary classification of loops based on presence or absence in –auxin/+auxin led to some misclassified looping changes. For example, there were cases when a loop was not called in +auxin yet still showed a similar signal as in –auxin. The discrepancy in loop calls could be due to a loop falling slightly below the threshold of detection in one condition despite showing minimal signal change. Therefore, we used a stricter characterization of loops based on quantitative change in loop strength rather than presence or absence in conditions.

To quantify looping change after auxin treatment, we calculated $\log_2(+\text{auxin loop strength}/-\text{auxin loop strength})$. We annotated looping change based on a 1.5-FC threshold. Loops with change $>\log_2(1.5)$ as ‘strengthened’, change $<-\log_2(1.5)$ as ‘weakened’ and all other loops as ‘unchanged’.

The same steps mentioned above were applied again to call and quantify loops in synchronized mid G1 samples (that is, a separate loop list was generated for mid G1 contact maps).

Statistics and reproducibility

No statistical method was used to predetermine the sample size. We used sample sizes consistent with ENCODE standards for genome-wide sequencing experiments. Two to three biological replicates were used for ChIP-seq, four to five biological replicates for Micro-C and three biological replicates for RNA-seq and TT-seq. One late G1 Pol II ChIP-seq (YY1–AID –auxin) replicate was excluded due to low ChIP signal and identification as an outlier in principal component analysis. No other samples were excluded from the analysis. The experiments were not randomized. The investigators were not blinded to allocation during experiments and outcome assessment.

Additional methods are described in the Supplementary Methods.

Reporting summary

Further information on research design is available in the Nature Portfolio Reporting Summary linked to this article.

Data availability

The raw and processed Micro-C, ChIP-seq, RNA-seq and TT-seq data generated from this study are deposited in the Gene Expression Omnibus (GEO) database under accession [GSE247254](#). External CTCF–AID Hi-C data from a previous study²⁴ are available at [GSE168251](#). External SMC3–AID Hi-C data from a previous study⁸⁴ are available at [GSE228402](#). External mitosis-to-G1 Hi-C and ChIP-seq data from a previous study⁶⁷ are available at [GSE129997](#). Source data are provided with this paper.

Code availability

The code used in this study is available at https://github.com/jclqrslam_2024_Code and <https://zenodo.org/doi/10.5281/zenodo.11992254>.

References

113. Rylski, M. et al. GATA-1-mediated proliferation arrest during erythroid maturation. *Mol. Cell. Biol.* **23**, 5031–5042 (2003).
114. Lam, J. *jclqr/Lam_2024_Code*: v1.0.0 (v1.0.0). Zenodo 10.5281/zenodo.11992255 (2024).
115. Langmead, B., Wilks, C., Antonescu, V. & Charles, R. Scaling read aligners to hundreds of threads on general-purpose processors. *Bioinformatics* **35**, 421–432 (2018).
116. Langmead, B. & Salzberg, S. L. Fast gapped-read alignment with Bowtie 2. *Nat. Methods* **9**, 357–359 (2012).
117. Danecek, P. et al. Twelve years of SAMtools and BCFtools. *GigaScience* **10**, giab008 (2021).
118. Feng, J., Liu, T., Qin, B., Zhang, Y. & Liu, X. S. Identifying ChIP-seq enrichment using MACS. *Nat. Protoc.* **7**, 1728–1740 (2012).
119. Ross-Innes, C. S. et al. Differential oestrogen receptor binding is associated with clinical outcome in breast cancer. *Nature* **481**, 389–393 (2012).
120. Quinlan, A. R. & Hall, I. M. BEDTools: a flexible suite of utilities for comparing genomic features. *Bioinformatics* **26**, 841–842 (2010).
121. Dale, R. K., Pedersen, B. S. & Quinlan, A. R. Pybedtools: a flexible Python library for manipulating genomic datasets and annotations. *Bioinformatics* **27**, 3423–3424 (2011).
122. Love, M. I., Huber, W. & Anders, S. Moderated estimation of fold change and dispersion for RNA-seq data with DESeq2. *Genome Biol.* **15**, 550 (2014).
123. Heinz, S. et al. Simple combinations of lineage-determining transcription factors prime cis-regulatory elements required for macrophage and B cell identities. *Mol. Cell* **38**, 576–589 (2010).
124. Ramírez, F. et al. deepTools2: a next generation web server for deep-sequencing data analysis. *Nucleic Acids Res.* **44**, W160–W165 (2016).
125. Zhu, A., Ibrahim, J. G. & Love, M. I. Heavy-tailed prior distributions for sequence count data: removing the noise and preserving large differences. *Bioinformatics* **35**, 2084–2092 (2018).
126. Xu, W. et al. CoolBox: a flexible toolkit for visual analysis of genomics data. *BMC Bioinformatics* **22**, 489 (2021).

Acknowledgements

The authors would like to thank E. Nora, E. Joyce and members of the Blobel Laboratory for helpful discussions. The authors would also like

to thank the Children’s Hospital of Philadelphia Flow Cytometry Core for technical assistance with cell sorting. This work was supported by grants T32GM007170, T32HG000046 and F30DK132824 (to J.C.L.), T32GM008216 and the Blavatnik Family Fellowship Award (to N.G.A.), R24DK106766 (to R.C.H. and G.A.B.), National Science Foundation of China (grant 32100422 to H.Z.) and R01DK054937, R01DK058044 and U01DK127405 (to G.A.B.).

Author contributions

J.C.L. and G.A.B. conceived the study. J.C.L., N.G.A. and S.C.M. performed the Micro-C experiments. J.C.L. and S.C.M. performed cell synchronization and ChIP experiments. S.W. performed the TT-seq experiments and sequencing alignment. J.C.L. and A.H. generated the YY1-AID cell line. K.A.H. performed RT-qPCR validation. C.A.K., B.G. and R.C.H. prepared ChIP-seq and RNA-seq libraries and performed sequencing and preprocessed sequencing data. J.C.L. analyzed all datasets and interpreted the results. N.G.A. and H.Z. helped with the interpretation of results. J.C.L. and G.A.B. wrote the manuscript with input from all authors.

Competing interests

The authors declare no competing interests.

Additional information

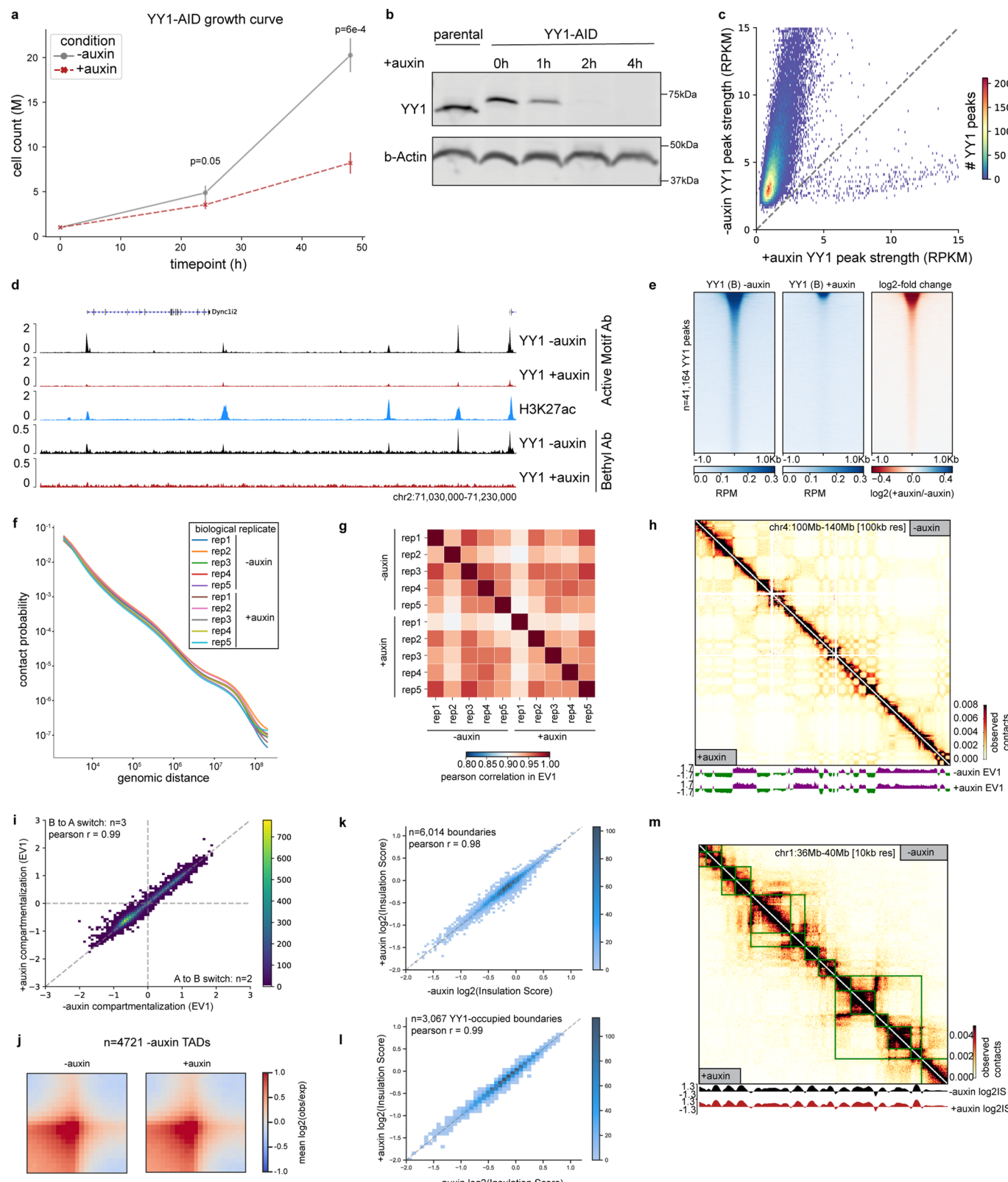
Extended data is available for this paper at <https://doi.org/10.1038/s41588-024-01871-y>.

Supplementary information The online version contains supplementary material available at <https://doi.org/10.1038/s41588-024-01871-y>.

Correspondence and requests for materials should be addressed to Gerd A. Blobel.

Peer review information *Nature Genetics* thanks Guillaume Andrey, Bas van Steensel and the other, anonymous, reviewer(s) for their contribution to the peer review of this work.

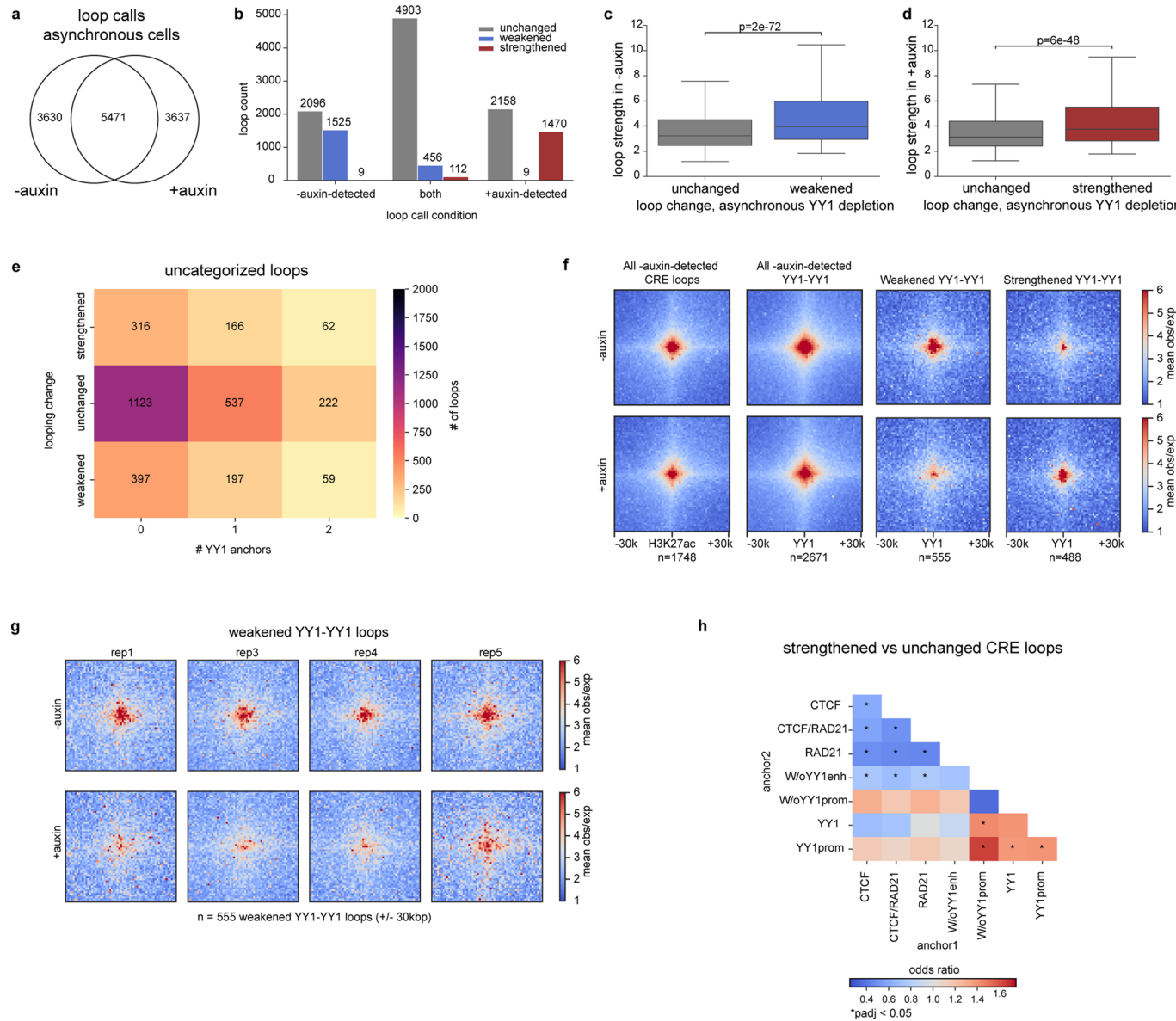
Reprints and permissions information is available at www.nature.com/reprints.



Extended Data Fig. 1 | See next page for caption.

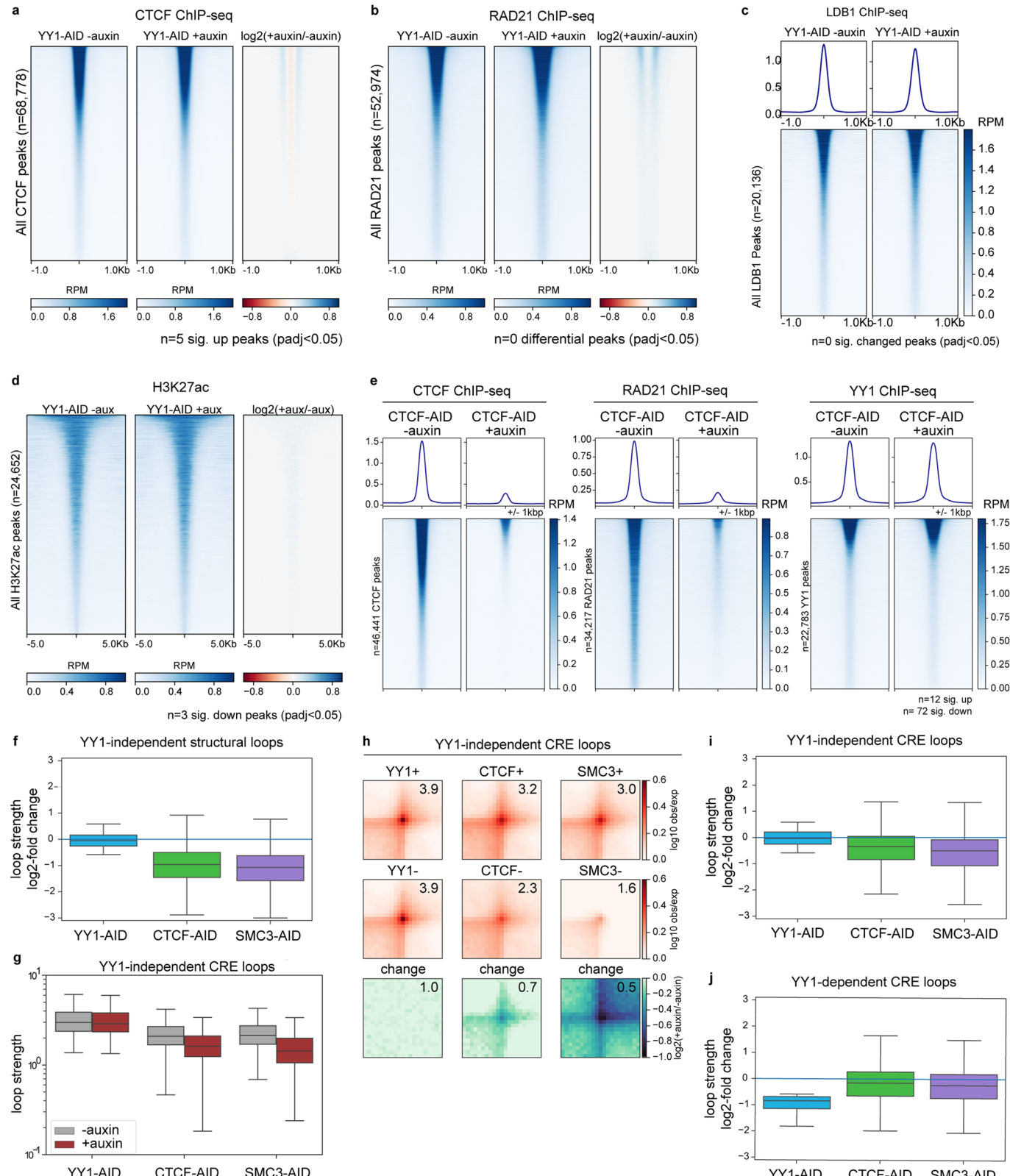
Extended Data Fig. 1 | Compartments and domains are maintained in the absence of YY1. **a**, YY1-AID cell counts for –auxin and +auxin conditions. Results are shown as mean \pm s.d. ($n = 3$ biological replicates, two-sided independent t-test). **b**, Western blot for YY1 in parental cells and YY1-AID cells after an auxin time-course. **c**, Histogram of YY1 ChIP-seq signal at YY1 peaks for –auxin and +auxin conditions. **d**, ChIP-seq tracks for YY1 (Active Motif antibody), YY1 (Bethyl antibody) and H3K27ac from –auxin and +auxin conditions. **e**, Heatmaps of YY1 ChIP-seq signal (Bethyl antibody) and mean \log_2 -fold change (+auxin/-auxin) centered on all YY1 peaks ($n = 2$ biological replicates). **f**, Micro-C contact versus distance curves for each biological replicate. **g**, Heatmap of Pearson correlations of compartment eigenvector 1 values (EV1) between biological replicates. **h**, Micro-C contact maps from –auxin (top) and

+auxin (bottom) conditions along with tracks of compartment EV1, with positive values corresponding to A compartment and negative values corresponding to B compartment. **i**, Histogram of EV1 values from –auxin and +auxin contact maps ($n = 25,257$ bins). **j**, Aggregate domain plot for all domains called in the –auxin contact map, centered on upstream and downstream boundaries. **k**, Histogram of \log_2 insulation score values from –auxin and +auxin contact maps for all boundaries called across both conditions. **l**, Histogram of \log_2 insulation score values from –auxin and +auxin contact maps for the subset of boundaries that have YY1 binding within ± 50 kb. **m**, Micro-C contact maps from –auxin (top) and +auxin (bottom) conditions, annotated with example TAD calls. Corresponding tracks show \log_2 insulation scores (IS).



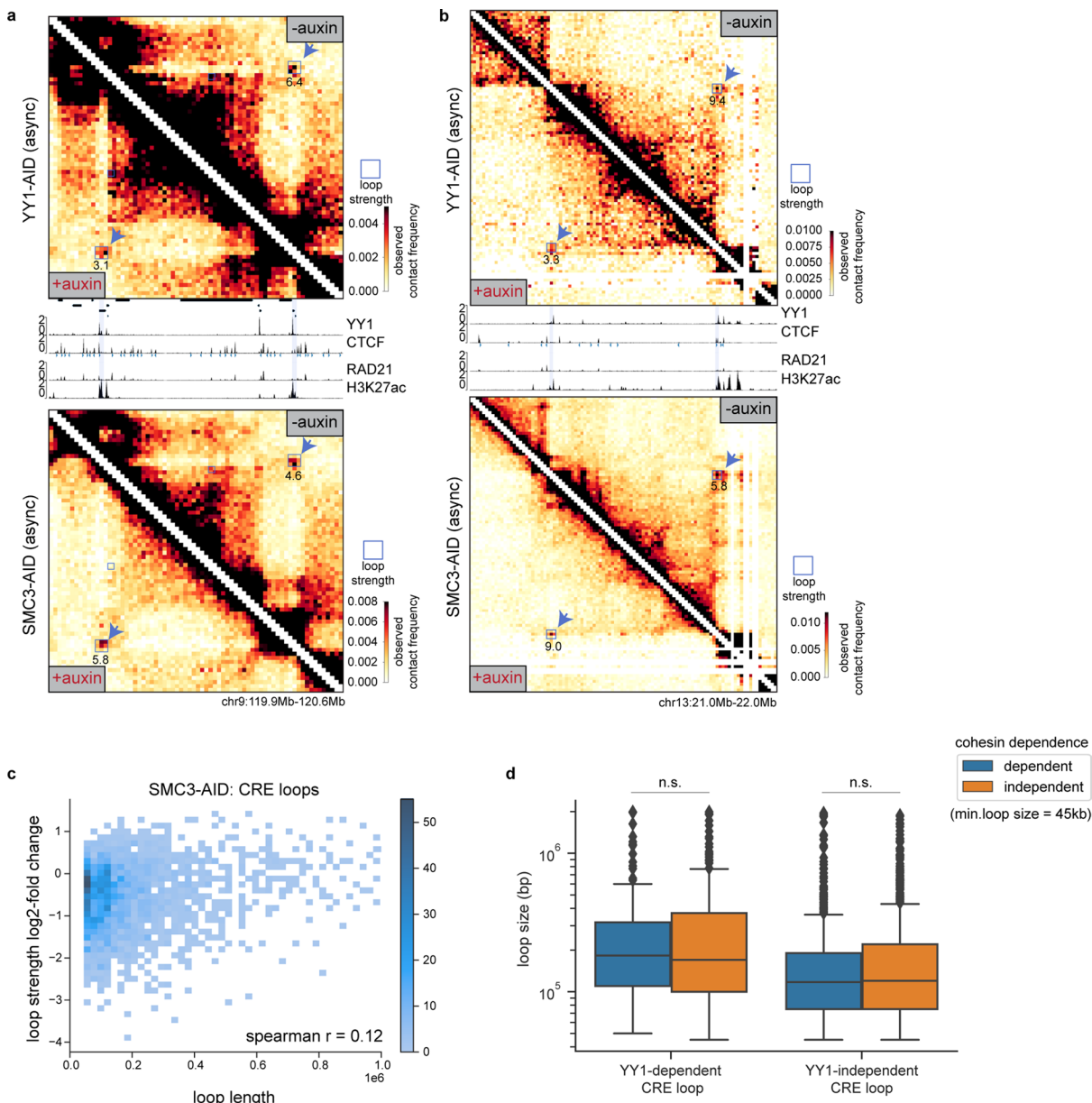
Extended Data Fig. 2 | Chromatin loop changes after YY1 depletion in asynchronous cells. **a**, Venn diagram of loop calls from –auxin and +auxin contact maps. **b**, Bar plot of loop change counts, stratified by the condition in which the loop was called. **c**, Box plot of loop strengths in the –auxin contact map, stratified by loop change (two-sided Mann–Whitney *U* test). **d**, Box plot of loop strengths in the +auxin contact map, stratified by loop change (two-sided Mann–Whitney *U* test). **e**, Counts of uncategorized loops across categories of looping change and YY1 occupancy. **f**, Pileup plots of all H3K27ac-H3K27ac loops.

and YY1-YY1 loops detected in the –auxin condition, weakened YY1-YY1 loops and strengthened YY1-YY1 loops (1 kb resolution, ± 30 kb window). **g**, Pileup plots of weakened YY1-YY1 loops for individual biological replicates. Loops are centered on YY1 ChIP-seq peaks ($n = 555$ loops, 1 kb resolution, ± 30 kb window). **h**, Enrichment of different factor occupancy patterns in strengthened CRE loops (* $p_{adj} < 0.05$, two-sided Fisher’s exact test, Benjamini–Hochberg multiple testing correction).



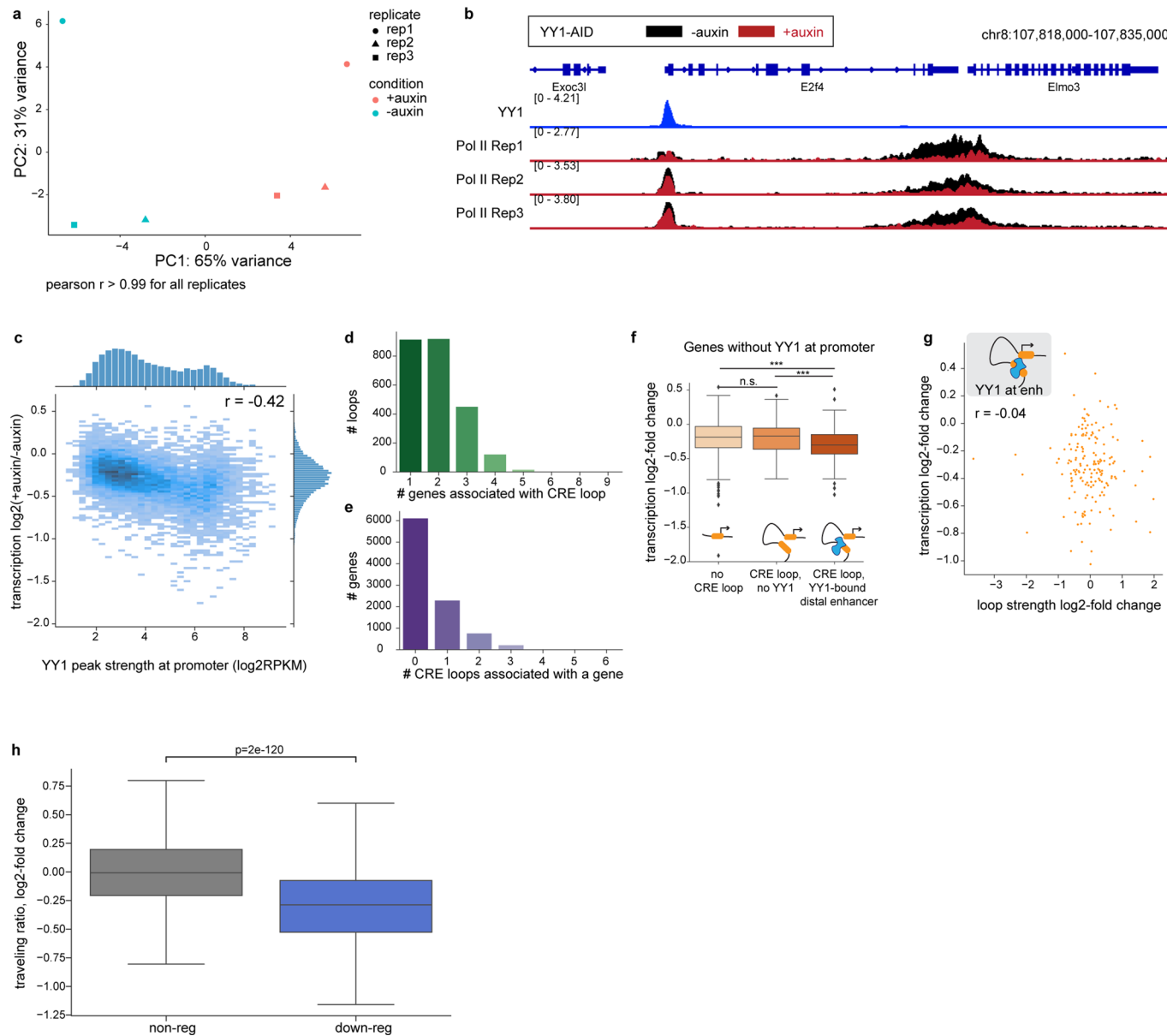
Extended Data Fig. 3 | CTCF, cohesin and LDB1 peaks remain stable upon YY1 depletion. **a**, Heatmaps showing CTCF ChIP-seq signal at all CTCF peaks before and after YY1 depletion in asynchronous cells. **b**, Heatmaps showing RAD21 ChIP-seq signal at all RAD21 peaks before and after asynchronous YY1 depletion. **c**, Heatmaps showing LDB1 ChIP-seq signal at all LDB1 peaks before and after YY1 depletion in asynchronous cells. **d**, Heatmaps showing H3K27ac ChIP-seq signal at all H3K27ac peaks before and after YY1 depletion in asynchronous cells. **e**, Heatmaps showing CTCF, RAD21 and YY1 ChIP-seq signal at their respective peaks before and after CTCF depletion in asynchronous cells. **f**, Box plot of loop strength fold changes of YY1-independent structural loops after YY1, CTCF or SMC3 depletion. **g**, Box plot of loop strengths of YY1-independent CRE loops after YY1, CTCF or SMC3 degradation. **h**, Pileup plots of YY1-AID, CTCF-AID and SMC3-AID contact maps. **i**, Box plot of loop strength fold changes of YY1-independent CRE loops after YY1, CTCF or SMC3 depletion. **j**, Box plot of loop strength fold changes of YY1-dependent CRE loops after YY1, CTCF or SMC3 depletion.

strength fold changes of YY1-independent structural loops after YY1, CTCF or SMC3 depletion. **g**, Box plot of loop strengths of YY1-independent CRE loops after YY1, CTCF or SMC3 degradation. **h**, Pileup plots of YY1-AID, CTCF-AID and SMC3-AID contact maps. **i**, Box plot of loop strength fold changes of YY1-independent CRE loops after YY1, CTCF or SMC3 depletion. **j**, Box plot of loop strength fold changes of YY1-dependent CRE loops after YY1, CTCF or SMC3 depletion.



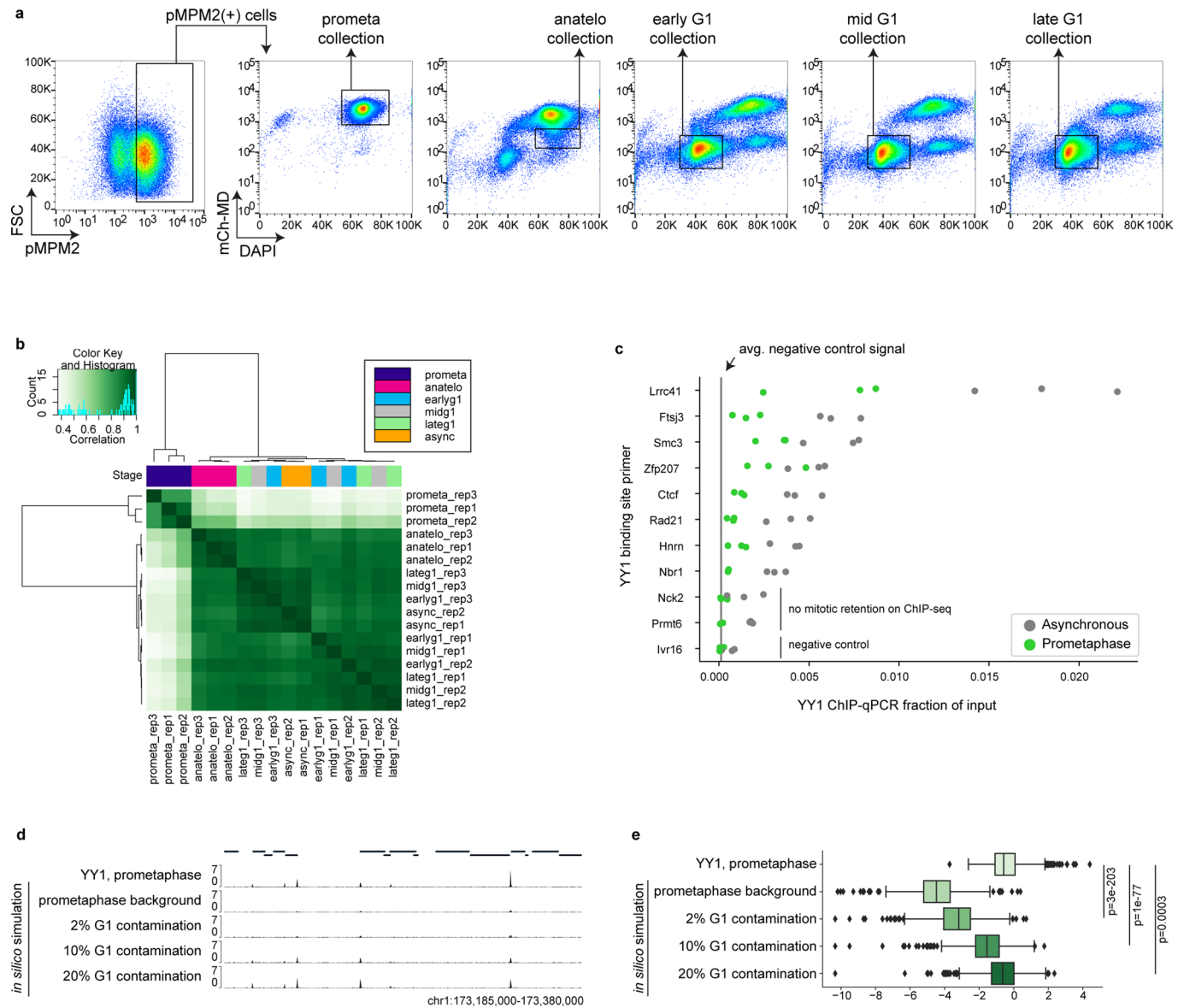
Extended Data Fig. 4 | Examples of YY1-dependent loops after cohesin depletion. **a,** Contact maps showing an example of a YY1-dependent loop (blue arrows) that persists after SMC3 depletion. Upper heatmap shows interactions before/after YY1 depletion, and lower heatmap shows interactions before/after SMC3 depletion. Tracks show YY1, CTCF, RAD21 and H3K27ac ChIP-seq

in untreated YY1-AID cells. **b**, A different example of a YY1-dependent loop that persists after SMC3 depletion. **c**, Histogram plot displaying CRE loop length versus the \log_2 -fold change in loop strength after cohesin depletion in asynchronous cells. **d**, Box plot displaying CRE loop lengths, stratified for cohesin-dependence and YY1 dependence (two-sided Mann-Whitney U test)



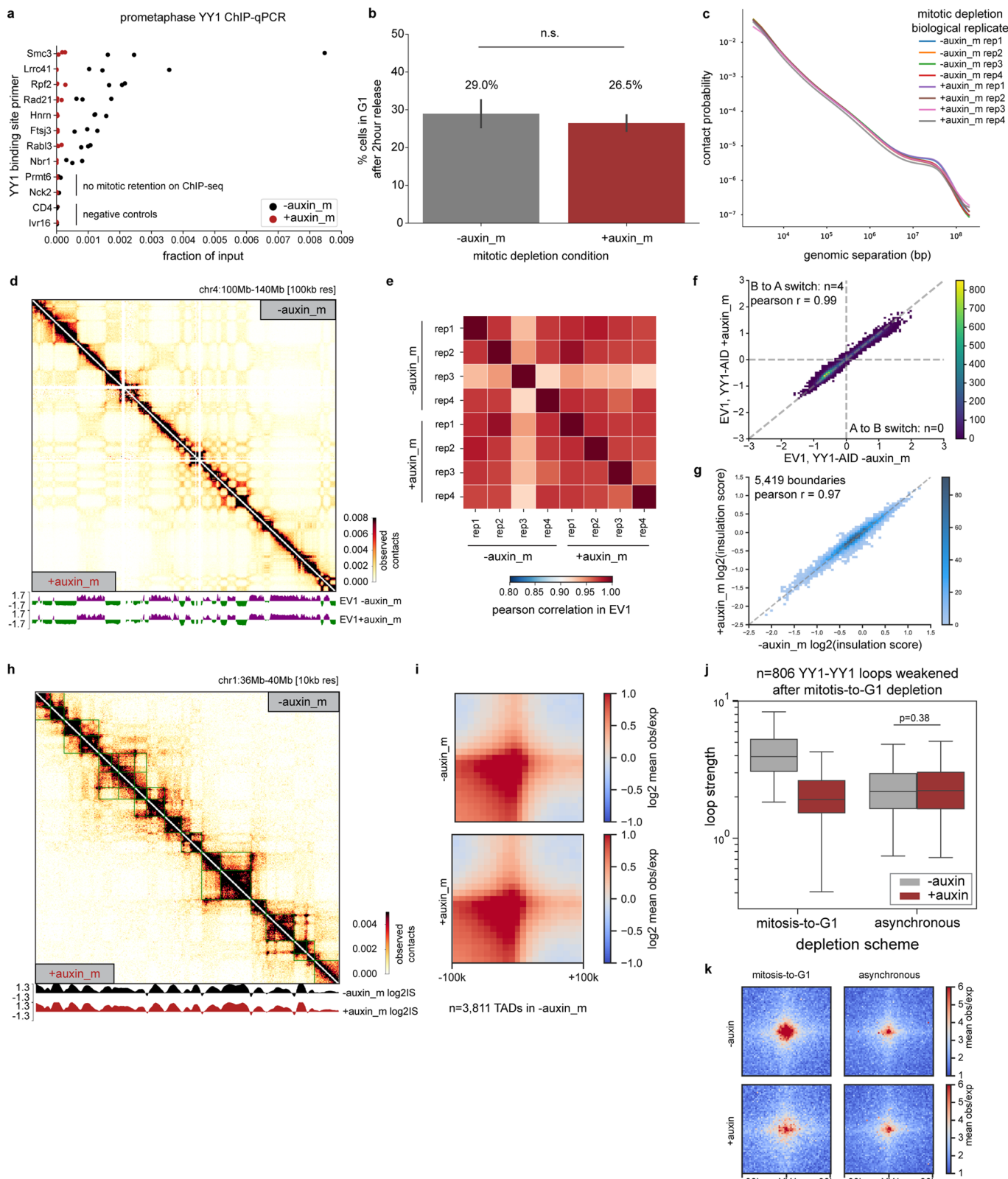
Extended Data Fig. 5 | Maintenance of transcription requires continuous presence of YY1. **a**, Principal component analysis (PCA) of individual biological replicates of Pol II ChIP-seq. **b**, Representative tracks of RPM-normalized YY1 ChIP-seq from untreated YY1-AID cells and Pol II ChIP-seq before/after YY1 depletion from biological replicates of asynchronous cells. **c**, Histogram plot showing transcription change for genes versus YY1 peak strength at gene promoters (Spearman correlation coefficient = -0.41). **d**, Histogram of the multiplicity of active genes associated with CRE loops. **e**, Histogram of the multiplicity of CRE loops associated with active genes. **f**, Box plot showing

transcription changes for different looping configurations at genes that do not have YY1 binding at the promoter (two-sided Mann–Whitney U test; from top to bottom: $p = 1e-7$, $p = 1e-4$, $p = 0.28$). **g**, Scatter plot showing loop strength change versus transcription change in asynchronous YY1-AID at loops that have YY1 at the distal enhancer but not at the promoter (Spearman correlation coefficient = 0.003). **h**, Box plot showing \log_2 -fold change in traveling ratio for genes after YY1 depletion in asynchronous cells (two-sided Mann–Whitney U test).



Extended Data Fig. 6 | YY1 chromatin binding dynamics during the mitosis-to-G1 transition. **a**, Representative plots of the gating strategy for purification of mitosis-to-G1 populations. **b**, Heatmap showing the Pearson correlation in YY1 occupancy between biological replicates of YY1 ChIP-seq for mitosis-to-G1 stages. **c**, YY1 ChIP-qPCR in asynchronous (async) cells and synchronized/sorted prometaphase cells. Primers, labeled with the nearest or overlapping gene,

include YY1 binding sites that display mitotic retention as well as sites that have no mitotic retention on ChIP-seq ($n = 3$ biological replicates). **d**, Prometaphase YY1 ChIP-seq track plotted alongside in silico generated tracks simulating prometaphase background and various levels of interphase contamination. **e**, Box plot showing YY1 binding at retained peaks genome-wide for different levels of simulated interphase contamination (two-sided Mann-Whitney U test).



Extended Data Fig. 7 | See next page for caption.

Extended Data Fig. 7 | Compartmentalization and TAD establishment following YY1 depletion. **a**, YY1 ChIP-qPCR of synchronized, sorted prometaphase cells after mitosis-to-G1 depletion of YY1 ($n = 3$ biological replicates). **b**, Bar plot of the percent of cells in G1 after 2-hour release from nocodazole arrest after mitosis-to-G1 depletion of YY1, as assessed by DAPI signal from flow cytometry (two-sided Mann–Whitney U test). **c**, Micro-C contact probability curves for all biological replicates. **d**, Representative Micro-C contact maps with tracks of compartmentalization, with positive eigenvector 1 values (EV1) corresponding to A compartment and negative values corresponding to B compartment. **e**, Heatmap of Pearson correlations of subcompartment

eigenvector 1 (EV1) values between biological replicates. **f**, Histogram plot of EV1 values after mitosis-to-G1 depletion. **g**, Histogram of \log_2 insulation score values for all boundaries detected in the –auxin_m contact map. **h**, Representative Micro-C contact map annotated with example TAD calls. Tracks show \log_2 insulation score values. **i**, Aggregate domain plot for all TADs called in control contact map, centered on upstream and downstream boundaries. **j**, Box plot showing loop strengths of all mid G1-detected YY1–YY1 loops weakened by mitosis-to-G1 depletion of YY1 (two-sided Mann–Whitney U test). **k**, Pileup plots corresponding to loops included in **j**.

Reporting Summary

Nature Portfolio wishes to improve the reproducibility of the work that we publish. This form provides structure for consistency and transparency in reporting. For further information on Nature Portfolio policies, see our [Editorial Policies](#) and the [Editorial Policy Checklist](#).

Statistics

For all statistical analyses, confirm that the following items are present in the figure legend, table legend, main text, or Methods section.

n/a Confirmed

- The exact sample size (n) for each experimental group/condition, given as a discrete number and unit of measurement
- A statement on whether measurements were taken from distinct samples or whether the same sample was measured repeatedly
- The statistical test(s) used AND whether they are one- or two-sided
 - Only common tests should be described solely by name; describe more complex techniques in the Methods section.*
- A description of all covariates tested
- A description of any assumptions or corrections, such as tests of normality and adjustment for multiple comparisons
- A full description of the statistical parameters including central tendency (e.g. means) or other basic estimates (e.g. regression coefficient) AND variation (e.g. standard deviation) or associated estimates of uncertainty (e.g. confidence intervals)
- For null hypothesis testing, the test statistic (e.g. F , t , r) with confidence intervals, effect sizes, degrees of freedom and P value noted
 - Give P values as exact values whenever suitable.*
- For Bayesian analysis, information on the choice of priors and Markov chain Monte Carlo settings
- For hierarchical and complex designs, identification of the appropriate level for tests and full reporting of outcomes
- Estimates of effect sizes (e.g. Cohen's d , Pearson's r), indicating how they were calculated

Our web collection on [statistics for biologists](#) contains articles on many of the points above.

Software and code

Policy information about [availability of computer code](#)

Data collection For flow data collection, we used the software Summit v6.3 (Beckman Coulter).

Data analysis For flow cytometry analysis, we used FlowJo v10.8.1.

Code used in this study is available at https://github.com/jclqrs/Lam_2024_Code and at <https://zenodo.org/doi/10.5281/zenodo.11992254>.

Software and package versions used for sequencing data analysis and figure generation are detailed in the Methods.

For manuscripts utilizing custom algorithms or software that are central to the research but not yet described in published literature, software must be made available to editors and reviewers. We strongly encourage code deposition in a community repository (e.g. GitHub). See the Nature Portfolio [guidelines for submitting code & software](#) for further information.

Data

Policy information about [availability of data](#)

All manuscripts must include a [data availability statement](#). This statement should provide the following information, where applicable:

- Accession codes, unique identifiers, or web links for publicly available datasets
- A description of any restrictions on data availability
- For clinical datasets or third party data, please ensure that the statement adheres to our [policy](#)

The raw and processed Micro-C, RNA-seq, TT-seq, and ChIP-seq data generated from this study are deposited in the GEO database under accession number GSE247254. External CTCF-AID Hi-C data from a previous study is available at GSE168251. External mitosis-to-G1 phase Hi-C and ChIP-seq data from a previous study is available at GSE129997. External SMC3-AID Hi-C data from a previous study is available at GSE228402.

Research involving human participants, their data, or biological material

Policy information about studies with [human participants or human data](#). See also policy information about [sex, gender \(identity/presentation\), and sexual orientation](#) and [race, ethnicity and racism](#).

Reporting on sex and gender

N/A

Reporting on race, ethnicity, or other socially relevant groupings

N/A

Population characteristics

N/A

Recruitment

N/A

Ethics oversight

N/A

Note that full information on the approval of the study protocol must also be provided in the manuscript.

Field-specific reporting

Please select the one below that is the best fit for your research. If you are not sure, read the appropriate sections before making your selection.

Life sciences

Behavioural & social sciences

Ecological, evolutionary & environmental sciences

For a reference copy of the document with all sections, see nature.com/documents/nr-reporting-summary-flat.pdf

Life sciences study design

All studies must disclose on these points even when the disclosure is negative.

Sample size

We used sample sizes consistent with ENCODE standards for replicates. We used 2-3 biological replicates for ChIP-seq, 4-5 biological replicates for Micro-C, and 3 biological replicates for TT-seq and RNA-seq.

Data exclusions

One late G1 Pol2 ChIP-seq (YY1-AID -auxin) replicate was excluded because it had low ChIP signal and was identified as an outlier in principal component analysis.

Replication

Attempts at replication were successful.

Randomization

Experiments did not include any treatments that could be randomized.

Blinding

Our study did not include any experiments where blinding was necessary.

Reporting for specific materials, systems and methods

We require information from authors about some types of materials, experimental systems and methods used in many studies. Here, indicate whether each material, system or method listed is relevant to your study. If you are not sure if a list item applies to your research, read the appropriate section before selecting a response.

Materials & experimental systems

n/a	Involved in the study
<input type="checkbox"/>	<input checked="" type="checkbox"/> Antibodies
<input type="checkbox"/>	<input checked="" type="checkbox"/> Eukaryotic cell lines
<input checked="" type="checkbox"/>	<input type="checkbox"/> Palaeontology and archaeology
<input checked="" type="checkbox"/>	<input type="checkbox"/> Animals and other organisms
<input checked="" type="checkbox"/>	<input type="checkbox"/> Clinical data
<input checked="" type="checkbox"/>	<input type="checkbox"/> Dual use research of concern
<input checked="" type="checkbox"/>	<input type="checkbox"/> Plants

Methods

n/a	Involved in the study
<input type="checkbox"/>	<input checked="" type="checkbox"/> ChIP-seq
<input type="checkbox"/>	<input checked="" type="checkbox"/> Flow cytometry
<input checked="" type="checkbox"/>	<input type="checkbox"/> MRI-based neuroimaging

Antibodies

Antibodies used

anti-Pol II Rpb1 NTD D8L4Y (Cell Signaling 14958), Dilution: 10uL/ChIP
 anti-YY1 (Active Motif 61779), Dilution: 10ug/ChIP
 anti-YY1 (Bethyl A302-779A), Dilution: 10ug/ChIP, 1:2000 for western blot
 anti-b-actin (Santa Cruz sc-47778), Dilution: 1:500 for western blot
 anti-RAD21 (Abcam ab992), Dilution: 10ug/ChIP
 anti-CTCF (Millipore 07-729), Dilution: 10uL/ChIP
 anti-H3K27ac (Active Motif 39133), Dilution: 10ug/ChIP
 anti-pMPM2 antibody (Millipore 05-368), Dilution: 0.5uL/10 million cells
 APC-conjugated F(ab')2-Goat anti-Mouse secondary antibody (Thermo Fisher Scientific 17-4010-82), Dilution: 2uL/10million cells
 anti-CLIM2 antibody (Santa Cruz sc-365074), Dilution: 10ug/ChIP

Validation

anti-pMPM2 Millipore 05-368 - This antibody has been tested in our cell line and validated to stain mitotic cells in FACS-based experiments (Campbell et al., 2014, *Biotechniques*).

F(ab')2-goat anti-mouse secondary antibody, APC, Thermo Fisher Scientific, 17-4010-82 - The manufacturer has tested this antibody to be suitable for immunofluorescence studies.

anti-CTCF Millipore 07-729. This antibody has been validated for ChIP-seq by the manufacturer - This antibody was also extensively used for ChIP-seq studies and demonstrates loss of signal upon CTCF depletion in our hands and by others (e.g.. Nora. et al. 2017).

anti-Rad21 Abcam ab992 - This antibody has been validated for ChIP experiments by the manufacturer. This antibody also demonstrated signal loss upon loss of Rad21 (Rao. et al. 2017).

anti-Pol II Cell Signaling 14958 - This antibody has been validated for ChIP by the manufacturer. This antibody has also been previously used in our lab (Behera et al. 2019, *Cell Reports*) and by others for ChIP experiments (e.g., Sun Y. et al. 2019, *Science Advances*.)

anti-YY1 Active Motif 61779 - This antibody has been validated for ChIP by the manufacturer. Our lab and others (Hsieh et al., 2022, *Nature Genetics*) have demonstrated loss of signal upon YY1 depletion.

anti-YY1 (Bethyl A302-779A) - Our lab and others (Hsieh et al., 2022, *Nature Genetics*) have demonstrated loss of signal upon YY1 depletion.

anti-H3K27ac (Active Motif 39133) - This antibody has been validated for ChIP-seq by the manufacturer based on known positive and negative control sites in HAP1 cells. In our cell line ChIP-seq peaks coincide with active enhancers and promoters, as expected.

anti-CLIM2 antibody (Santa Cruz sc-365074) - Our lab has demonstrated ChIP-seq signal loss upon depletion of LDB1

Eukaryotic cell lines

Policy information about [cell lines and Sex and Gender in Research](#)

Cell line source(s)

The G1E-ER4 cell line was a gift from the Mitchell J Weiss laboratory at St. Jude Children's Hospital. The Drosophila Schneider 2 (S2) cell line was purchased from Gibco (R69007).

Authentication

We regularly confirm that these cells can be induced to undergo terminal erythroid differentiation.

Mycoplasma contamination

G1E-ER4 cells have been tested to be negative for Mycoplasma.

Commonly misidentified lines (See [ICLAC](#) register)

No commonly misidentified lines were used.

Plants

Seed stocks

Report on the source of all seed stocks or other plant material used. If applicable, state the seed stock centre and catalogue number. If plant specimens were collected from the field, describe the collection location, date and sampling procedures.

Novel plant genotypes

Describe the methods by which all novel plant genotypes were produced. This includes those generated by transgenic approaches, gene editing, chemical/radiation-based mutagenesis and hybridization. For transgenic lines, describe the transformation method, the number of independent lines analyzed and the generation upon which experiments were performed. For gene-edited lines, describe the editor used, the endogenous sequence targeted for editing, the targeting guide RNA sequence (if applicable) and how the editor was applied.

Authentication

Describe any authentication procedures for each seed stock used or novel genotype generated. Describe any experiments used to assess the effect of a mutation and, where applicable, how potential secondary effects (e.g. second site T-DNA insertions, mosaicism, off-target gene editing) were examined.

Data deposition

Confirm that both raw and final processed data have been deposited in a public database such as [GEO](#).

Confirm that you have deposited or provided access to graph files (e.g. BED files) for the called peaks.

Data access links

May remain private before publication.

<https://www.ncbi.nlm.nih.gov/geo/query/acc.cgi?acc=GSE247254>

Files in database submission

```

YY1aid_async_untreated.mcool
YY1aid_async_auxin.mcool
YY1aid_async_untreated_compartmentEV1.bw
YY1aid_async_auxin_compartmentEV1.bw
YY1aid_async_untreated_log2insulationscore.bw
YY1aid_async_auxin_log2insulationscore.bw
YY1aid_async_merged_boundaries.bed
YY1aid_async_merged_domains.bedpe
YY1aid_async_merged_loops.bedpe
YY1aid_mg1_untreated.mcool
YY1aid_mg1_auxin.mcool
YY1aid_mg1_compartmentEV1_untreated.bw
YY1aid_mg1_compartmentEV1_auxin.bw
YY1aid_mg1_untreated_log2insulationscore.bw
YY1aid_mg1_auxin_log2insulationscore.bw
YY1aid_mg1_merged_boundaries.bed
YY1aid_mg1_merged_domains.bedpe
YY1aid_midg1_merged_loops.bedpe
YY1aid_async_untreated_RAD21_chip.bw
YY1aid_async_untreated_YY1_chip.bw
YY1aid_async_untreated_CTCF_chip.bw
YY1aid_async_auxin_YY1_chip.bw
YY1aid_async_auxin_RAD21_chip.bw
YY1aid_async_auxin_CTCF_chip.bw
YY1aid_async_untreated_H3K27ac_chip.bw
YY1_prometa_chip.bw
YY1_earlyG1_chip.bw
YY1_anatelo_chip.bw
YY1_lateG1_chip.bw
YY1_prometa_chip.bw
YY1aid_async_untreated_RAD21_peaks.bed
YY1aid_async_untreated_CTCF_peaks.bed
YY1aid_async_untreated_YY1_peaks.bed
YY1aid_async_auxin_YY1_peaks.bed
YY1aid_async_auxin_CTCF_peaks.bed
YY1aid_async_auxin_RAD21_peaks.bed
YY1aid_async_untreated_H3K27ac_peaks.bed
YY1_prometa-emergent_peaks.bed
YY1_lateg1-emergent_peaks.bed
YY1_earlyg1-emergent_peaks.bed
YY1_anatelo-emergent_peaks.bed
YY1_midg1-emergent_peaks.bed
YY1aid_asyn_auxin_Pol2_chip.bw
YY1aid_asyn_untreated_Pol2_chip.bw
YY1aid_midG1_auxin_Pol2_chip.bw
YY1aid_earlyG1_auxin_Pol2_chip.bw
YY1aid_midG1_untreated_Pol2_chip.bw

```

YY1aid_earlyG1_untreated_Pol2_chip.bw
YY1aid_lateG1_untreated_Pol2_chip.bw
YY1aid_lateG1_auxin_Pol2_chip.bw
input_YY1aid_async_auxin.bw
input_YY1aid_async_untreated.bw
input_YY1aid_earlyg1_auxin.bw
input_YY1aid_earlyg1_untreated.bw
input_YY1aid_lateg1_auxin.bw
input_YY1aid_lateg1_untreated.bw
input_YY1aid_midg1_auxin.bw
input_YY1aid_midg1_untreated.bw
YY1aid_async_auxin YY1b.bw
YY1aid_async_auxin YY1b_peaks.bed
YY1aid_async_untreated YY1b.bw
YY1aid_async_untreated YY1b_peaks.bed
YY1_async_chip.bw
3634_S3_L001_R1_001.fastq.gz
3635_S4_L001_R1_001.fastq.gz
3778_S2_L001_R1_001.fastq.gz
3779_S3_L001_R1_001.fastq.gz
3823_S5_L001_R1_001.fastq.gz
3823_S1_R1_001.fastq.gz
3824_S6_L001_R1_001.fastq.gz
3824_S2_R1_001.fastq.gz
3825_S7_L001_R1_001.fastq.gz
3825_S3_R1_001.fastq.gz
3826_S8_L001_R1_001.fastq.gz
3826_S4_R1_001.fastq.gz
4057_S3_R1_001.fastq.gz
4058_S4_R1_001.fastq.gz
4055_S1_R1_001.fastq.gz
4056_S2_R1_001.fastq.gz
3906_S5_R1_001.fastq.gz
3906_S6_R1_001.fastq.gz
3907_S6_R1_001.fastq.gz
3907_S7_R1_001.fastq.gz
3908_S7_R1_001.fastq.gz
3908_S8_R1_001.fastq.gz
3909_S8_R1_001.fastq.gz
3909_S9_R1_001.fastq.gz
3632_S1_L001_R1_001.fastq.gz
3632_S1_R1_001.fastq.gz
3633_S2_L001_R1_001.fastq.gz
3635_S1_R1_001.fastq.gz
3634_S2_R1_001.fastq.gz
3633_S2_R1_001.fastq.gz
4351_S7_R1_001.fastq.gz
4352_S8_R1_001.fastq.gz
4353_S9_R1_001.fastq.gz
4354_S10_R1_001.fastq.gz
4355_S11_R1_001.fastq.gz
4356_S12_R1_001.fastq.gz
4397_S7_R1_001.fastq.gz
4398_S8_R1_001.fastq.gz
4399_S9_R1_001.fastq.gz
4400_S10_R1_001.fastq.gz
4401_S11_R1_001.fastq.gz
4402_S12_R1_001.fastq.gz
4210_S15_R1_001.fastq
4211_S16_R1_001.fastq
4167_S1_R1_001.fastq.gz
4168_S2_R1_001.fastq.gz
4212_S17_R1_001.fastq.gz
4213_S18_R1_001.fastq.gz
4214_S19_R1_001.fastq.gz
4215_S20_R1_001.fastq.gz
4196_S1_R1_001.fastq.gz
4197_S2_R1_001.fastq.gz
4198_S3_R1_001.fastq.gz
4199_S4_R1_001.fastq.gz
4200_S5_R1_001.fastq.gz
4201_S6_R1_001.fastq.gz
4584_S1_R1_001.fastq.gz
4585_S2_R1_001.fastq.gz
4586_S3_R1_001.fastq.gz
4587_S4_R1_001.fastq.gz

4588_S5_R1_001.fastq.gz
4589_S6_R1_001.fastq.gz
4590_S7_R1_001.fastq.gz
4591_S8_R1_001.fastq.gz
4592_S9_R1_001.fastq.gz
4593_S10_R1_001.fastq.gz
4594_S11_R1_001.fastq.gz
4595_S12_R1_001.fastq.gz
3668_S13_L001_R1_001.fastq.gz
3659_S4_L001_R1_001.fastq.gz
4640_S10_R1_001.fastq.gz
4642_S12_R1_001.fastq.gz
4644_S14_R1_001.fastq.gz
4646_S16_R1_001.fastq.gz
4208_y7none_S13_R1_001.fastq.gz
4209_y7auxin_S14_R1_001.fastq.gz
4205_early4_S10_R1_001.fastq.gz
4204_late0_S9_R1_001.fastq.gz
4206_mid4_S11_R1_001.fastq.gz
4207_late4_S12_R1_001.fastq.gz
4202_early0_S7_R1_001.fastq.gz
4203_mid0_S8_R1_001.fastq.gz
3479_S1_R1_001.fastq.gz
3480_S2_R1_001.fastq.gz
3481_S3_R1_001.fastq.gz
3852_S11_L001_R1_001.fastq.gz
3853_S12_L001_R1_001.fastq.gz
3854_S13_L001_R1_001.fastq.gz
3855_S14_L001_R1_001.fastq.gz
3856_S15_L001_R1_001.fastq.gz
3857_S16_L001_R1_001.fastq.gz
3858_S17_L001_R1_001.fastq.gz
4425_S1_R1_001.fastq.gz
4426_S2_R1_001.fastq.gz
4427_S3_R1_001.fastq.gz
4428_S4_R1_001.fastq.gz
4429_S5_R1_001.fastq.gz
4430_S6_R1_001.fastq.gz
4431_S7_R1_001.fastq.gz
run431_4055_S1_R1_001.fastq.gz
run431_4056_S2_R1_001.fastq.gz
run431_4057_S3_R1_001.fastq.gz
run431_4058_S4_R1_001.fastq.gz
3634_S3_L001_R2_001.fastq.gz
3635_S4_L001_R2_001.fastq.gz
3778_S2_L001_R2_001.fastq.gz
3779_S3_L001_R2_001.fastq.gz
3823_S5_L001_R2_001.fastq.gz
3823_S1_R2_001.fastq.gz
3824_S6_L001_R2_001.fastq.gz
3824_S2_R2_001.fastq.gz
3825_S7_L001_R2_001.fastq.gz
3825_S3_R2_001.fastq.gz
3826_S8_L001_R2_001.fastq.gz
3826_S4_R2_001.fastq.gz
4057_S3_R2_001.fastq.gz
4058_S4_R2_001.fastq.gz
4055_S1_R2_001.fastq.gz
4056_S2_R2_001.fastq.gz
3906_S5_R2_001.fastq.gz
3906_S6_R2_001.fastq.gz
3907_S6_R2_001.fastq.gz
3907_S7_R2_001.fastq.gz
3908_S7_R2_001.fastq.gz
3908_S8_R2_001.fastq.gz
3909_S8_R2_001.fastq.gz
3909_S9_R2_001.fastq.gz
3632_S1_L001_R2_001.fastq.gz
3632_S1_R2_001.fastq.gz
3633_S2_L001_R2_001.fastq.gz
3635_S1_R2_001.fastq.gz
3634_S2_R2_001.fastq.gz
3633_S2_R2_001.fastq.gz
4351_S7_R2_001.fastq.gz
4352_S8_R2_001.fastq.gz
4353_S9_R2_001.fastq.gz

4354_S10_R2_001.fastq.gz
4355_S11_R2_001.fastq.gz
4356_S12_R2_001.fastq.gz
4397_S7_R2_001.fastq.gz
4398_S8_R2_001.fastq.gz
4399_S9_R2_001.fastq.gz
4400_S10_R2_001.fastq.gz
4401_S11_R2_001.fastq.gz
4402_S12_R2_001.fastq.gz
4210_S15_R2_001.fastq
4211_S16_R2_001.fastq
4167_S1_R2_001.fastq.gz
4168_S2_R2_001.fastq.gz
4212_S17_R2_001.fastq.gz
4213_S18_R2_001.fastq.gz
4214_S19_R2_001.fastq.gz
4215_S20_R2_001.fastq.gz
4196_S1_R2_001.fastq.gz
4197_S2_R2_001.fastq.gz
4198_S3_R2_001.fastq.gz
4199_S4_R2_001.fastq.gz
4200_S5_R2_001.fastq.gz
4201_S6_R2_001.fastq.gz
4584_S1_R2_001.fastq.gz
4585_S2_R2_001.fastq.gz
4586_S3_R2_001.fastq.gz
4587_S4_R2_001.fastq.gz
4588_S5_R2_001.fastq.gz
4589_S6_R2_001.fastq.gz
4590_S7_R2_001.fastq.gz
4591_S8_R2_001.fastq.gz
4592_S9_R2_001.fastq.gz
4593_S10_R2_001.fastq.gz
4594_S11_R2_001.fastq.gz
4595_S12_R2_001.fastq.gz
4640_S10_R2_001.fastq.gz
4642_S12_R2_001.fastq.gz
4644_S14_R2_001.fastq.gz
4646_S16_R2_001.fastq.gz
4208_y7none_S13_R2_001.fastq.gz
4209_y7auxin_S14_R2_001.fastq.gz
4205_early4_S10_R2_001.fastq.gz
4204_late0_S9_R2_001.fastq.gz
4206_mid4_S11_R2_001.fastq.gz
4207_late4_S12_R2_001.fastq.gz
4202_early0_S7_R2_001.fastq.gz
4203_mid0_S8_R2_001.fastq.gz
3479_S1_R2_001.fastq.gz
3480_S2_R2_001.fastq.gz
3481_S3_R2_001.fastq.gz
3852_S11_L001_R2_001.fastq.gz
3853_S12_L001_R2_001.fastq.gz
3854_S13_L001_R2_001.fastq.gz
3855_S14_L001_R2_001.fastq.gz
3856_S15_L001_R2_001.fastq.gz
3857_S16_L001_R2_001.fastq.gz
3858_S17_L001_R2_001.fastq.gz
4425_S1_R2_001.fastq.gz
4426_S2_R2_001.fastq.gz
4427_S3_R2_001.fastq.gz
4428_S4_R2_001.fastq.gz
4429_S5_R2_001.fastq.gz
4430_S6_R2_001.fastq.gz
4431_S7_R2_001.fastq.gz
run431_4055_S1_R2_001.fastq.gz
run431_4056_S2_R2_001.fastq.gz
run431_4057_S3_R2_001.fastq.gz
run431_4058_S4_R2_001.fastq.gz
CTCFaid_async_auxin_YY1_chip.bw
CTCFaid_async_untreated_YY1_chip.bw
YY1aid_async_auxin_LDB1_chip.bw
YY1aid_async_untreated_LDB1_chip.bw
YY1aid_async_Auxin_H3K27ac_chip.bw
CTCFaid_async_auxin_YY1_peaks.bed
CTCFaid_async_untreated_YY1_peaks.bed
YY1aid_async_auxin_LDB1_peaks.bed

Methodology

Replicates

For CTCF, RAD21, LDB1, and H3K27ac ChIP-seq, we performed 2 biological replicates per condition.

For YY1 and PolII ChIP-seq, we performed 3 biological replicates per condition.

For YY1, we also performed 2 additional biological replicates per condition using an alternative antibody (anti-YY1 Bethyl A302-779A).

Sequencing depth

See Supplemental Table 5 for Micro-C 2x50bp paired-end sequencing statistics.

All ChIP-seq reads were 2x50bp paired-end sequenced, except for H3K27ac ChIP-seqs, which were single-end 1x75bp.

```

ChIP-seq sample,sequenced_reads,mapped_deduplicated_reads
YY1aid_async_untreated_YY1_ChIPseq_Rep1,31708932,17683904
YY1aid_async_untreated_CTCF_ChIPseq_Rep1,23255892,15675228
YY1aid_async_untreated_RAD21_ChIPseq_Rep1,30905683,20011669
YY1aid_async_auxin_YY1_ChIPseq_Rep1,31774508,18991887
YY1aid_async_auxin_CTCF_ChIPseq_Rep1,36596809,23976395
YY1aid_async_auxin_RAD21_ChIPseq_Rep1,30233955,18440797
YY1aid_async_untreated_YY1_ChIPseq_Rep2,33579260,18537082
YY1aid_async_untreated_CTCF_ChIPseq_Rep2,35330260,21715806
YY1aid_async_untreated_RAD21_ChIPseq_Rep2,31316107,18151465
YY1aid_async_auxin_YY1_ChIPseq_Rep2,29478394,15518274
YY1aid_async_auxin_CTCF_ChIPseq_Rep2,36878513,22942777
YY1aid_async_auxin_RAD21_ChIPseq_Rep2,46935163,26720516
YY1aid_async_untreated_YY1_ChIPseq_Rep3,45421595,23728197
YY1aid_async_auxin_YY1_ChIPseq_Rep3,44374460,14435171
YY1aid_async_untreated_Pol2_ChIPseq_rep1,24065192,13870969
YY1aid_async_auxin_Pol2_ChIPseq_rep1,32464042,14091255
YY1aid_async_untreated_Pol2_ChIPseq_rep2,45405201,26289681
YY1aid_async_auxin_Pol2_ChIPseq_rep2,44945201,25996449
YY1aid_async_untreated_Pol2_ChIPseq_rep3,45073172,27206634
YY1aid_async_auxin_Pol2_ChIPseq_rep3,51114574,29215935
YY1aid_earlyG1_untreated_Pol2_ChIPseq_rep3,40460549,14851948
YY1aid_midG1_untreated_Pol2_ChIPseq_rep3,35806557,17500651
YY1aid_lateG1_untreated_Pol2_ChIPseq_rep3,51639740,26696956
YY1aid_earlyG1_auxin_Pol2_ChIPseq_rep3,47528690,22273202
YY1aid_midG1_auxin_Pol2_ChIPseq_rep3,55236800,23218785
YY1aid_lateG1_auxin_Pol2_ChIPseq_rep3,42691977,17327835
YY1aid_earlyG1_untreated_Pol2_ChIPseq_rep1,34490764,17203787
YY1aid_earlyG1_auxin_Pol2_ChIPseq_rep1,34398194,18091012
YY1aid_midG1_untreated_Pol2_ChIPseq_rep1,38570288,19906721
YY1aid_midG1_auxin_Pol2_ChIPseq_rep1,30924361,15938618
YY1aid_lateG1_untreated_Pol2_ChIPseq_rep1,34951633,20325376
YY1aid_lateG1_auxin_Pol2_ChIPseq_rep1,35214595,18186245
YY1aid_earlyG1_untreated_Pol2_ChIPseq_rep2,36781770,21193731
YY1aid_earlyG1_auxin_Pol2_ChIPseq_rep2,36212697,17977055
YY1aid_midG1_untreated_Pol2_ChIPseq_rep2,35932573,19460955
YY1aid_midG1_auxin_Pol2_ChIPseq_rep2,32751229,18413306
YY1aid_lateG1_untreated_Pol2_ChIPseq_rep2,29116933,10120717
YY1aid_lateG1_auxin_Pol2_ChIPseq_rep2,39113671,21772230
YY1aid_async_untreated_H3K27ac_ChIPseq_rep1,36902425,22107128
YY1aid_async_untreated_H3K27ac_ChIPseq_rep2,41581866,24953643
YY1aid_async_auxin_YY1b_ChIPseq_rep1,26552375,15552245
YY1aid_async_untreated_YY1b_ChIPseq_rep1,33543115,20427465
YY1aid_async_untreated_YY1b_ChIPseq_rep2,25458102,16115553
YY1aid_async_auxin_YY1b_ChIPseq_rep2,28285884,16323106
YY1aid_async_untreated_input,36156059,22467681
YY1aid_async_auxin_input,36301024,22958344
YY1aid_earlyG1_auxin_input,42398692,25803558
YY1aid_lateG1_untreated_input,37399512,23116254
YY1aid_midG1_auxin_input,39118878,24163368
YY1aid_lateG1_auxin_input,50962037,30265398
YY1aid_earlyG1_untreated_input,27806204,17736556
YY1aid_midG1_untreated_input,35778300,21075069
G1E-ER4_earlyG1_YY1_ChIPseq_rep1,47049842,16859931
G1E-ER4_midG1_YY1_ChIPseq_rep1,49995943,11431247
G1E-ER4_lateG1_YY1_ChIPseq_rep1,33457047,11525512
G1E-ER4_prometa_YY1_ChIPseq_rep1,26655010,1525786
G1E-ER4_anatelo_YY1_ChIPseq_rep1,40494016,8951001
G1E-ER4_prometa_YY1_ChIPseq_rep2,27741815,3989064
G1E-ER4_anatelo_YY1_ChIPseq_rep2,32670126,5843966
G1E-ER4_earlyG1_YY1_ChIPseq_rep2,22368100,5344474
G1E-ER4_midG1_YY1_ChIPseq_rep2,24522139,7193245

```

ChIP-seq

YY1aid_asyncUntreated_LDB1_peaks.bed
YY1aid_asyncAuxin_H3K27ac_peaks.bed
YY1aid_asyncrep1_untreated_TTseq_spikenormed_for.bw
YY1aid_asyncrep1_auxin_TTseq_spikenormed_for.bw
YY1aid_asyncrep2_auxin_TTseq_spikenormed_for.bw
YY1aid_asyncrep2_untreated_TTseq_spikenormed_for.bw
YY1aid_asyncrep3_untreated_TTseq_spikenormed_rev.bw
YY1aid_asyncrep3_auxin_TTseq_spikenormed_rev.bw
YY1aid_asyncrep3_untreated_TTseq_spikenormed_for.bw
YY1aid_asyncrep1_auxin_TTseq_spikenormed_rev.bw
YY1aid_asyncrep2_auxin_TTseq_spikenormed_rev.bw
YY1aid_ttseq_spikein_counts_htseq.txt
YY1aid_ttseq_sample_counts_htseq.txt
4641_S11_R1_001.fastq.gz
4643_S13_R1_001.fastq.gz
4645_S15_R1_001.fastq.gz
4647_S17_R1_001.fastq.gz
4509_S13_R1_001.fastq.gz
4510_S14_R1_001.fastq.gz
4629_S7_R1_001.fastq.gz
4630_S8_R1_001.fastq.gz
3669_S14_L001_R1_001.fastq.gz
3660_S5_L001_R1_001.fastq.gz
4786_30Mreads_R1.fastq.gz
4787_30Mreads_R1.fastq.gz
4788_30Mreads_R1.fastq.gz
4789_30Mreads_R1.fastq.gz
4790_30Mreads_R1.fastq.gz
4791_30Mreads_R1.fastq.gz
4792_30Mreads_R1.fastq.gz
4793_30Mreads_R1.fastq.gz
4794_30Mreads_R1.fastq.gz
4795_30Mreads_R1.fastq.gz
4796_30Mreads_R1.fastq.gz
4797_30Mreads_R1.fastq.gz
4641_S11_R2_001.fastq.gz
4643_S13_R2_001.fastq.gz
4645_S15_R2_001.fastq.gz
4647_S17_R2_001.fastq.gz
4509_S13_R2_001.fastq.gz
4510_S14_R2_001.fastq.gz
4629_S7_R2_001.fastq.gz
4630_S8_R2_001.fastq.gz
4786_30Mreads_R2.fastq.gz
4787_30Mreads_R2.fastq.gz
4788_30Mreads_R2.fastq.gz
4789_30Mreads_R2.fastq.gz
4790_30Mreads_R2.fastq.gz
4791_30Mreads_R2.fastq.gz
4792_30Mreads_R2.fastq.gz
4793_30Mreads_R2.fastq.gz
4794_30Mreads_R2.fastq.gz
4795_30Mreads_R2.fastq.gz
4796_30Mreads_R2.fastq.gz
4797_30Mreads_R2.fastq.gz
4956_S1_R1_001.fastq.gz
4956_S1_R2_001.fastq.gz
4957_S2_R1_001.fastq.gz
4957_S2_R2_001.fastq.gz
4960_S1_R1_001.fastq.gz
4960_S1_R2_001.fastq.gz
4961_S2_R1_001.fastq.gz
4961_S2_R2_001.fastq.gz
4969_S6_R1_001.fastq.gz
4969_S6_R2_001.fastq.gz
5_TT_YY1_A-5min_0531.merged_R1_001.fastq.gz
5_TT_YY1_A-5min_0531.merged_R2_001.fastq.gz

Genome browser session
(e.g. [UCSC](#))

None

G1E-ER4_lateG1_YY1_ChIPseq_rep2,22815444,10514914
 G1E-ER4_prometa_YY1_ChIPseq_rep3,6336297,2327793
 G1E-ER4_anatelo_YY1_ChIPseq_rep3,36931320,7095065
 G1E-ER4_earlyg1_YY1_ChIPseq_rep3,41243382,9376470
 G1E-ER4_midg1_YY1_ChIPseq_rep3,32074426,9124069
 G1E-ER4_lateg1_YY1_ChIPseq_rep3,32402236,11386300
 G1E-ER4_async_YY1_ChIPseq_rep1,32135048,12384087
 G1E-ER4_async_YY1_ChIPseq_rep2,34805206,8174728
 YY1aid_async_auxin_H3K27ac_Rep1,40252839, 23754799
 YY1aid_async_auxin_H3K27ac_Rep2,43350924, 24637574
 YY1aid_async_untreated_LDB1_Rep1,28925523, 16854524
 YY1aid_async_untreated_LDB1_Rep2,27098559, 15243232
 YY1aid_async_auxin_LDB1_Rep1,26829496, 15617012
 YY1aid_async_auxin_LDB1_Rep2,23895232, 13888277
 CTCFaid_async_untreated_YY1_Rep1,18415828, 11607837
 CTCFaid_async_auxin_YY1_Rep1,27004770, 15901528
 CTCFaid_async_untreated_YY1_Rep2,33562067, 19519850
 CTCFaid_async_auxin_YY1_Rep2,33923367, 18998971

Antibodies

anti-Pol II Rpb1 NTD D8L4Y (Cell Signaling 14958), Dilution: 10uL/ChIP
 anti-YY1 (Active Motif 61779), Dilution: 10ug/ChIP
 anti-YY1 (Bethyl A302-779A), Dilution: 10ug/ChIP
 anti-RAD21 (Abcam ab992), Dilution: 10ug/ChIP
 anti-CTCF (Millipore 07-729), Dilution: 10uL/ChIP
 anti-H3K27ac (Active Motif 39133), Dilution: 10ug/ChIP
 anti-CLIM2 antibody (Santa Cruz sc-365074), Dilution: 10ug/ChIP

Peak calling parameters

We called narrow peaks for each replicate using macs2 (v2.2.7) callpeak with a condition-matched input file and peak-calling threshold of q=0.05.

Data quality

- (1) Sequencing quality was assessed with FastQC (v0.11.9)
- (2) Prior to peak calling, reads were de-duplicated and alignments with MAPQ < 20 were filtered out.
- (3) Correlation among peak calls was assessed for replicates.
- (4) Peaks of RAD21 and CTCF were largely overlapping. Motif analysis revealed underlying YY1 and CTCF motifs at peaks, as expected.
- (5) Pol II signal was located at expected genomic regions (TSS, gene bodies).

Software

For ChIP-seq data processing and analysis, we used bowtie2 (v2.2.5), SAMtools (v1.14), deeptools (v3.5.1), macs2 (v2.2.7), DiffBind (v3.5), pybedtools (0.8.2), and DESeq2 (v1.32.0), homer (v4.11.1).

Flow Cytometry

Plots

Confirm that:

- The axis labels state the marker and fluorochrome used (e.g. CD4-FITC).
- The axis scales are clearly visible. Include numbers along axes only for bottom left plot of group (a 'group' is an analysis of identical markers).
- All plots are contour plots with outliers or pseudocolor plots.
- A numerical value for number of cells or percentage (with statistics) is provided.

Methodology

Sample preparation

See Methods for detailed description of sample preparation. Briefly, G1E-ER4 cells were treated with nocodazole to synchronize them in prometaphase. To enrich for cells in ana/telophase, early G1, mid G1, and late G1, arrested cells were washed, resuspended in nocodazole-free media and released from prometaphase for 0.5h, 1h, 2h, and 4h. At each timepoint, cells were harvested, cross-linked, and stained for cell cycle markers.

Instrument

Beckman Coulter MoFlo Astrios EQ

Software

Flow plots were generated using FlowJo v10.8.1.

Cell population abundance

We typically obtained > 95% viable cells based on FSC-A and SSC-A.

Gating strategy

Prometaphase samples were sorted based on positive pMPM2, positive mCherry-MD, and 4N DAPI signal. Ana/telophase samples were sorted based on reduced mCherry-MD and 4N DAPI signal. Early G1, mid G1, and late G1 samples were sorted based on negative mCherry-MD and 2N DAPI signal.

- Tick this box to confirm that a figure exemplifying the gating strategy is provided in the Supplementary Information.